Cell Metabolism

Article

Peroxidation of n-3 and n-6 polyunsaturated fatty acids in the acidic tumor environment leads to ferroptosis-mediated anticancer effects

Graphical abstract

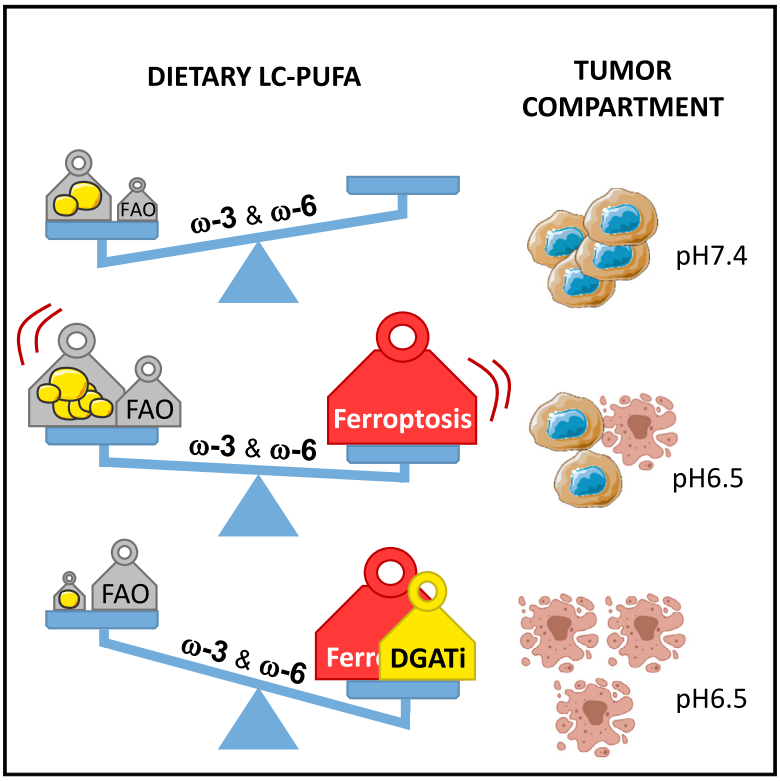

Highlights

- n-3 and n-6 PUFAs preferentially accumulate in lipid droplets of acidic cancer cells
- Excess LC-PUFAs undergo peroxidation and induce ferroptosis in acidic cancer cells
- DGAT inhibitors prevent the formation of lipid droplets and promote ferroptosis
- DGATi enhance the tumor growth inhibitory effects of dietary n-3 LC-PUFAs in mice

Authors

Emeline Dierge, Elena Debock, Céline Guilbaud, ..., Chantal Dessy, Yvan Larondelle, Olivier Feron

Correspondence

olivier.feron@uclouvain.be

In brief

Tumor acidosis is associated with the metabolic use of fatty acids. Dierge et al. describe that in acidic cancer cells, n-3 and n-6 LC-PUFAs that exceed lipid droplet storage capacity undergo peroxidation and induce ferroptosis. Antitumor effects of dietary n-3 LC-PUFAs are further increased upon administration of DGAT inhibitors.

Dierge et al., 2021, Cell Metabolism *33*, 1–15
August 3, 2021
https://doi.org/10.1016/j.cmet.2021.05.016

CellPress

Cell Metabolism

CellPress

Article

Peroxidation of n-3 and n-6 polyunsaturated fatty acids in the acidic tumor environment leads to ferroptosis-mediated anticancer effects

Emeline Dierge,[1,2] Elena Debock,[2] Céline Guilbaud,[1] Cyril Corbet,[1] Eric Mignolet,[2] Louise Mignard,[2] Estelle Bastien,[1] Chantal Dessy,[1] Yvan Larondelle,[2,3] and Olivier Feron[1,3,4,*]

[1]Pole of Pharmacology and Therapeutics (FATH), Institut de Recherche Expérimentale et Clinique (IREC), UCLouvain, 57 Avenue Hippocrate B1.5704, 1200 Brussels, Belgium

[2]Louvain Institute of Biomolecular Science and Technology (LIBST), UCLouvain, Croix du Sud 4-5/L7.07.03, 1348 Louvain-la-Neuve, Belgium

[3]These authors contributed equally

[4]Lead contact

*Correspondence: olivier.feron@uclouvain.be

https://doi.org/10.1016/j.cmet.2021.05.016

SUMMARY

Tumor acidosis promotes disease progression through a stimulation of fatty acid (FA) metabolism in cancer cells. Instead of blocking the use of FAs by acidic cancer cells, we examined whether excess uptake of specific FAs could lead to antitumor effects. We found that n-3 but also remarkably n-6 polyunsaturated FA (PUFA) selectively induced ferroptosis in cancer cells under ambient acidosis. Upon exceeding buffering capacity of triglyceride storage into lipid droplets, n-3 and n-6 PUFA peroxidation led to cytotoxic effects in proportion to the number of double bonds and even more so in the presence of diacylglycerol acyltransferase inhibitors (DGATi). Finally, an n-3 long-chain PUFA-rich diet significantly delayed mouse tumor growth when compared with a monounsaturated FA-rich diet, an effect further accentuated by administration of DGATi or ferroptosis inducers. These data point out dietary PUFA as a selective adjuvant antitumor modality that may efficiently complement pharmacological approaches.

INTRODUCTION

The contribution of different nutrients to biosynthetic, bioenergetic, and antioxidant needs of cancer cells has been extensively studied in the last decade (Vander Heiden and DeBerardinis, 2017). In particular, the relationship between cancer genetics and metabolism rewiring has led to major discoveries, offering new therapeutic perspectives for specific cancer types (Luengo et al., 2017; Tajan and Vousden, 2020). In many of these studies, the availability in the whole diversity of nutrients has been considered unlimited, cancer cells getting what they need according to mutation- and microenvironment-driven metabolic preferences (Davidson et al., 2016; DeNicola and Cantley, 2015; Muir et al., 2018; Palm and Thompson, 2017). Today, however, investigators are increasingly raising the question of whether diet may influence cancer progression through the modulation of the access to and the utilization of nutrients by tumor cells (Lien and Vander Heiden, 2019; Mayne et al., 2016; Steck and Murphy, 2020; Sullivan et al., 2019). The existing literature addressing this issue is contradictory with highly significant tumor growth inhibitory effects in response to specific diets but also quite drastic changes in dietary options leading to poor, if not counterproductive, effects on mouse tumor progression (Hopkins et al., 2018; Xia et al., 2017). Most of these dietary studies are based on the original idea that reducing tumor supply of major nutrients could limit cancer cell proliferation. Calorie restriction most often through a low carbohydrate content and more recently diets excluding specific amino acids have been investigated (Dierge et al., 2020; Lv et al., 2014). Applications of these approaches in cancer patients, including via the ketogenic diet that makes fat-generating ketone bodies to spare healthy organs, face obvious issues including weight loss, associated fatigue, and weakness together with practical difficulties in implementing these diets in an everyday cancer patient's life (Dierge and Feron, 2019; Nestle, 2018).

Strategies aiming to supplement specific nutrients instead of restricting diets are less numerous. Recent studies have identified dietary histidine (Kanarek et al., 2018) and mannose (Gonzalez et al., 2018) supplementations as promising low-risk interventions, but dietary omega-3 (n-3) polyunsaturated fatty acids (PUFAs) have along the years attracted the most attention for their potential anticancer effects. Outcomes of PUFA administration in tumor-bearing mice are indeed promising (see Dierge et al., 2020 for review). However, while transferability of dietary PUFAs to humans is easier to handle than calorie-restricted diets, clinical validation of potential benefits is still in its infancy, with a small number of trials, limited enrollment of patients, and confusion in data interpretation arising from variability in the PUFA nature, amount, and mode of administration (Berquin et al., 2008; Serini et al., 2016). Still, studies performed on cohort of >1,000 patients with colorectal

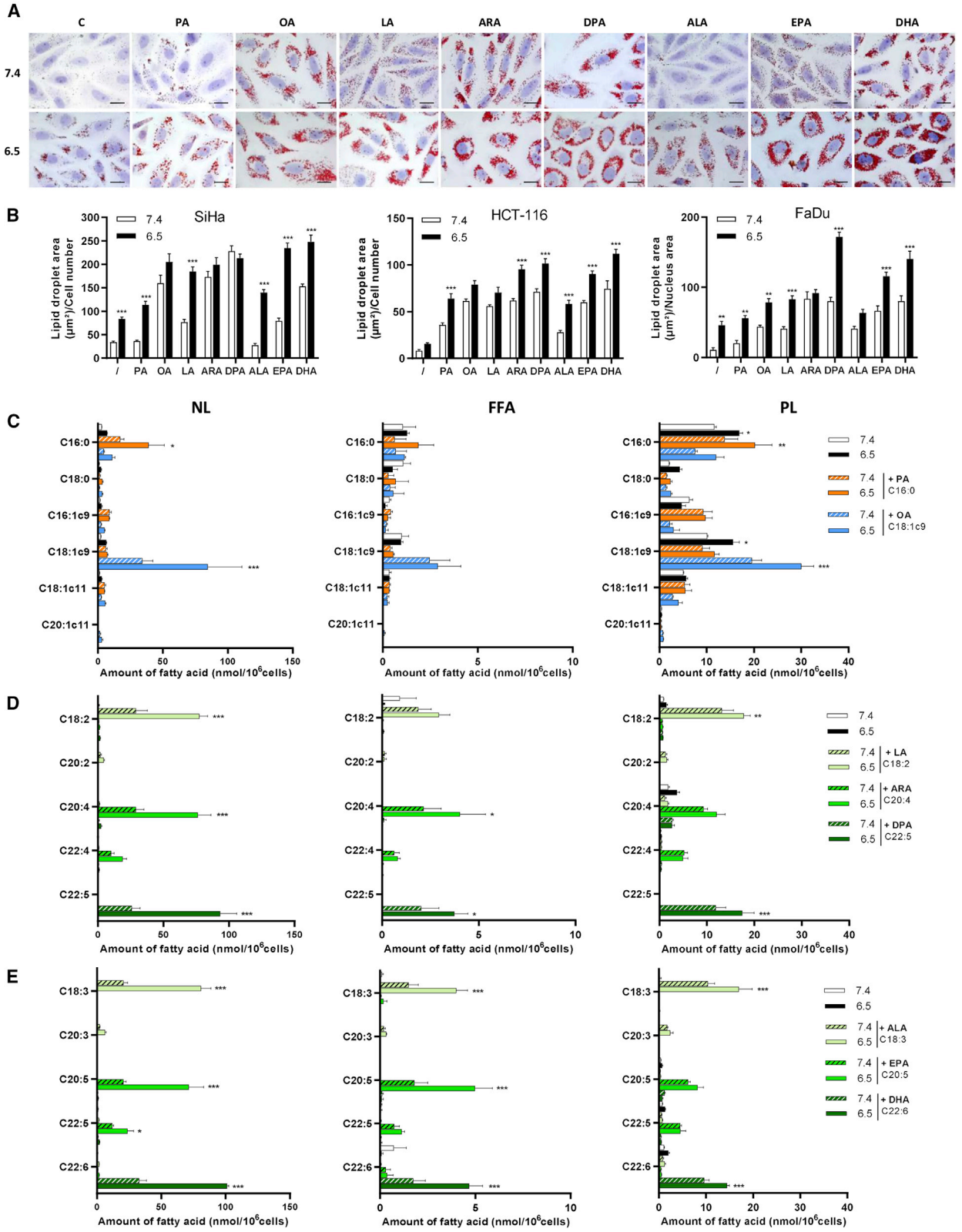

Figure 1. n-3 and n-6 PUFAs preferentially accumulate into lipid droplets of acidic cancer cells

(A and B) Representative pictures (A) (6.5/ and 7.4/SiHa cells) and quantification (B) of ORO-stained LDs in the pH 6.5-adapted SiHa, HCT-116, and FaDu cancer cells and corresponding cells maintained at pH 7.4 upon exposure for 24 h to 100 μM FAs including SFAs (palmitate, PA), MUFAs (oleate, OA), and PUFAs (n-6:

(legend continued on next page)

cancer revealed that higher intake of marine n-3 PUFAs after diagnosis is associated with lower cancer-associated deaths and longer disease-free survival (Van Blarigan et al., 2018; van der Meij et al., 2012). Different mechanisms are suggested based on *in vitro* studies including lipid peroxidation, apoptosis induction, but also direct anti-inflammatory signaling through G protein-coupled receptors (D'Eliseo and Velotti, 2016; Dierge and Feron, 2019). These pleiotropic effects, however, question the selectivity of action of PUFAs toward tumors (versus healthy organs). Indeed, while anti-inflammatory effects may not hurt, lipid peroxidation and associated cell death may represent potential adverse effects. A response to the selectivity issue of PUFAs may, however, arise from independent studies that in the last decade have documented a major role of lipid metabolism in tumor growth (Corbet and Feron, 2017; Snaebjornsson et al., 2020). Various reports have actually revealed that cancer cell growth was highly dependent in some mouse tumor models on fatty acid (FA) uptake and oxidation. We have previously reported that tumor acidosis, in particular, was associated with a profound rewiring of FA metabolism with glutamine acting as an FA precursor (Corbet et al., 2014, 2016), while concomitantly, uptake of exogenous FAs supported beta-oxidation and accumulation of triglycerides into lipid droplets (LDs) (Corbet et al., 2020). Moreover, we showed that these LDs serve as a source of FAs that could be mobilized and oxidized to fulfill cellular needs during the invasion process (Corbet et al., 2020).

In this study, we postulated that the increased FA uptake capacity of acidic cancer cells could account for a preferential delivery of PUFAs into this specific tumor compartment and thus for tumor-specific cytotoxic effects. We found that n-3 but also remarkably n-6 PUFAs induced cell death in 2D-grown acid-adapted cancer cells and within the acidic compartment of 3D tumor spheroids, the toxicity gradually increasing with the number of double bonds. The prior accumulation of both n-3 and n-6 PUFAs into LDs to a larger extent than that of saturated FAs (SFAs) and monounsaturated FAs (MUFAs) led us to suspect that storage of excess FAs into triglycerides was actually a strategy to mask double bonds from peroxidation. We further proved that peroxidability potential was increased in acidic cancer cells and that long-chain (LC) n-3 and n-6 PUFA peroxidation and consecutive ferroptosis accounted for the observed antitumor effects. Finally, we documented in mice that an n-3 LC-PUFA-rich diet led to a significant delay in tumor growth when compared with an MUFA-rich diet. Importantly, both *in vitro* and *in vivo* anticancer effects of LC-PUFAs were further increased upon administration of inhibitors of diacylglycerol acyltransferases to prevent PUFA buffering into LDs. Altogether, these data identify dietary LC-PUFA as an adjuvant modality to take advantage of acidosis-driven induction of ferroptosis in tumors.

RESULTS

n-3 and n-6 PUFAs preferentially accumulate into lipid droplets of acidic cancer cells

We first compared the capacity of acid-adapted cancer cells (6.5/cells) and corresponding cells maintained at neutral pH (7.4/cells) to capture FAs into LDs, including SFAs (palmitate, PA), MUFAs (oleate, OA), and PUFAs (n-6: linoleate, LA; arachidonate, ARA; docosapentaenoate, DPA; n-3: alpha-linolenate, ALA; eicosapentaenoate, EPA; docosahexaenoate, DHA). A global increase in LD accumulation of either FA was observed in 6.5/tumor cells of different origins, namely cervix (SiHa), colorectal (HCT-116), and hypopharyngeal (FaDu) cancer cell lines (Figures 1A, 1B, and S1A). It is noteworthy that 6.5/FaDu cells exhibited a net reduction in cell size (Figure S1A) so that the increase in LD area was normalized per nucleus area (Figure 1B). Interestingly, within the n-3 and n-6 PUFA series, we observed an increase in the size and number of LDs in proportion to the number of double bonds (n-6 series: C22:5, DPA > C20:4, ARA > C18:2, LA; n-3 series: C22:6, DHA > C20:5, EPA > C18:3, ALA) (Figures 1A, 1B, and S1A). These findings indicate that enhanced LD formation upon exposure to both n-3 and n-6 PUFAs directly reflects intracellular PUFA accumulation. As a further support to this observation, we showed that LD formation upon exposure to DHA was significantly reduced by blocking antibodies directed against CD36 that we recently identified as the main entry path for FAs under acidosis (Corbet et al., 2020) (Figure S1B).

We further carried out a gas chromatography-flame ionization detection (GC-FID)-based quantification of captured FAs as phospholipids (PLs), neutral lipids (NLs), or free FAs (FFAs). We first observed that each added FA accounted for a higher accumulation in 6.5/cancer cells than in 7.4/cancer cells (Figures 1C–1E and S2A–S2D). This difference was more pronounced within the NL and FFA fractions than in the PL fraction (Figures 1C–1E and S2B–S2D). The contribution of each added FA to the total amounts of NL revealed that both n-3 and n-6 PUFA series largely accumulated in 6.5/cancer cells in proportion to the number of double bonds (Figures S1C and S2A, left panels), thereby recapitulating the observed profile of LD accumulation. Higher amounts of C22:4 and C22:5 metabolites were also observed in the NL and FFA fractions of 6.5/cells exposed to n-6 C20:4 (ARA) and n-3 C20:5 (EPA), respectively (Figures 1D, 1E, S2C, and S2D), indicating elongase activity. 6.5/FaDu cells showed a 2- to 3-fold lesser accumulation of PL in response to added FAs (versus 7.4/FaDu cells) (Figures S3A–S3D, right panels), in agreement with the observed significant reduction in cell size under acidosis. When applying this correcting factor to the amounts of NL and FFA measured in 6.5/FaDu cells (Figures S3A–S3D), enrichment in either fraction was actually similar to that observed in 6.5/HCT-116 and 6.5/SiHa cancer cells.

linoleate, LA; arachidonate, ARA; docosapentaenoate, DPA; n-3: alpha-linolenate, ALA; eicosapentaenoate, EPA and docosahexaenoate, DHA). Scale bar, 20 μm.

(C–E) FA composition of neutral lipid (NL), free FA (FFA), and phospholipid (PL) fractions isolated from 6.5/ and 7.4/HCT-116 cells upon exposure to 100 μM PA and OA (C), n-6 PUFAs (LA, ARA, or DPA) (D), and n-3 PUFAs (ALA, EPA, or DHA) (E). A color code is associated with each added FA and its potential metabolite(s); FA amounts in lipid fractions from untreated 7.4/and 6.5/HCT-116 cells are indicated in white and black, respectively.

Data are represented as mean ± SEM of 10 pictures (B) or 3 independent experiments (C–E). Significance was determined by two-way ANOVA with Tukey's multiple comparison test. *$p < 0.05$; **$p < 0.01$; ***$p < 0.001$. See also Figure S1.

Please cite this article in press as: Dierge et al., Peroxidation of n-3 and n-6 polyunsaturated fatty acids in the acidic tumor environment leads to ferroptosis-mediated anticancer effects, Cell Metabolism (2021), https://doi.org/10.1016/j.cmet.2021.05.016

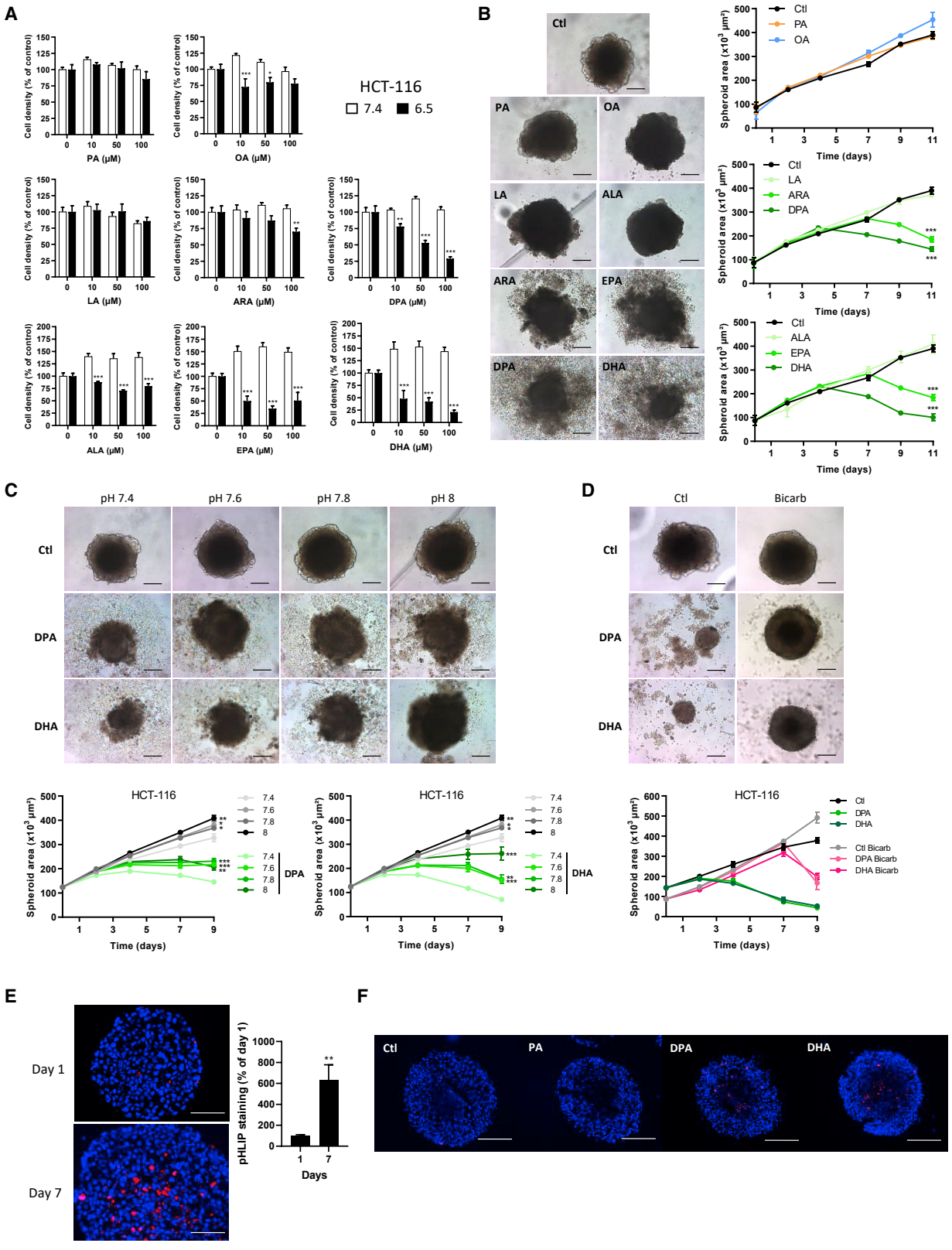

Figure 2. n-3 and n-6 PUFAs exert selective cytotoxic effects under acidosis

(A–D) Effects of the indicated FAs (see Figure 1 legend for abbreviations) on the growth of pH 6.5-adapted and pH 7.4-cultured HCT-116 cancer cells (A), as well as on the growth of 3D tumor spheroids generated from HCT-116 cancer cells (B). FAs were added at the indicated concentrations for 72 h in the indicated cancer

(legend continued on next page)

n-3 but also n-6 PUFAs exert selective cytotoxic effects in acidic cancer cells

While measurements of FA uptake and accumulation presented in Figure 1 were obtained after 24-h exposure and were not associated with significant cell death, longer exposure differently altered cell growth. We actually found that while PA and OA exposure did not lead to significant inhibition of cell growth, both n-3 and n-6 PUFAs dose-dependently inhibited cell growth in 6.5/cancer cells, but not in corresponding 7.4/cancer cells (Figures 2A, S4A, and S4B). The reduction in cancer cell growth was actually directly proportional to the number of double bonds in the n-3 PUFAs (C22:6, DHA > C20:5, EPA > C18:3, ALA) and remarkably also in the n-6 series (C22:5, DPA > C20:4, ARA > C18:2, LA), indicating that the observed antitumor effects were unlikely to be related to the formation of eicosanoids (known to exert anti- and pro-inflammatory effects according to their n-3 and n-6 origin, respectively).

To further examine the cytotoxic effects of PUFAs in a model wherein acidosis develops naturally, we used 3D tumor spheroids generated from the same FaDu and HCT-116 cancer cells as above; SiHa cells were not used here because they do not spontaneously form spheroids. In the HCT-116 and FaDu spheroids, effects of PUFAs once again followed the number of double bonds with DHA and DPA, leading to more dramatic growth inhibition than ARA and EPA (mainly detectable in HCT-116 spheroids) while LA and ALA had no or minimal impact (Figures 2B and S4C). Interestingly, no signs of toxicity could be observed in the first 3 days of spheroid exposure to PUFAs (i.e., a period that is yet associated with growth inhibition of cancer cells maintained at pH 6.5 in 2D culture conditions). The cytotoxic effects were actually observed from days 5 to 7 post-exposure to PUFAs (Figures 2B and S4C), a delay that could correspond to the time required for spontaneous acidosis to develop in the center of the spheroids. To validate this hypothesis, we first repeated the above experiments by culturing 3D tumor spheroids in a medium buffered at more alkaline pH. We found that the increased pH_e from 7.4 to 8 was associated with a progressive reduction in the growth inhibitory effects of both DHA and DPA (Figures 2C and S5A). We next used media containing 22 mM bicarbonate to neutralize H^+ generated by growing spheroids and observed the abrogation of the cytotoxic effects of both DPA and DHA (Figures 2D and S5B). In parallel, we used the acidic pH reporter pHLIP conjugated to AlexaFluor 568 dye and found that while no pHLIP staining was detected in spheroids with a mean diameter $\leq$600 μm, the marker confirmed the development of acidosis in the core of the spheroids at later stages (Figure 2E). Remarkably, using propidium iodide (PI) to detect cell death, we found that cells located at the center of the spheroids were the first to die after the exposure to DPA or DHA (but not PA), further supporting a major role of acidosis in the development of PUFA-mediated cytotoxicity (Figure 2F). Also, the presence of 22 mM bicarbonate in the extracellular medium strongly reduced pHLIP staining in 3D spheroids (Figure S5C) as well as the extent of PI-positive cells in the core of the spheroids exposed to DPA or DHA (Figure S5D).

n-3 and n-6 PUFAs preferentially induce lipid peroxidation under acidosis

Since the cytotoxic effects of n-3 and n-6 PUFAs under acidosis were observed in proportion to the number of double bonds, we next examined whether lipid peroxidation could account for the deleterious effects of PUFAs. Using BODIPY 581/591 undecanoic acid as a peroxidation sensor (Figure 3A), we found that 6.5/cancer cells exhibited an increased oxidation ability (versus corresponding 7.4/cancer cells) (Figure 3A). Malondialdehyde (MDA) measurements confirmed an increase in the lipid peroxidation pattern of acid-adapted cancer cells (Figure 3B). We then exposed both 6.5/ and 7.4/cancer cells to various FAs and examined the extent of generated MDA. While MDA levels were similar in either cell phenotype upon exposure to PA, OA, LA, and ALA, a net increase in MDA was observed in 6.5/cancer cells in the presence of n-3 EPA and DHA as well as n-6 ARA and DPA (Figures 3C, S6A, and S6B). The use of CD36-blocking antibodies confirmed that enhanced DHA uptake from the extracellular medium largely contributed to the increase in MDA levels (Figure 3D).

Cytotoxic effects of n-3 and n-6 PUFAs under acidosis result from ferroptosis

To better understand the nature of cell death induced by n-3 and n-6 PUFAs in acidic cancer cells, annexin V/PI staining was carried out and analyzed by flow cytometry. These experiments revealed a very limited transition through the annexin-V-positive, PI-negative quadrant before reaching the double-positive quadrant, suggesting a non-apoptotic mode of cell death (Figures S6C–S6E). The lack of caspase-3 cleavage further confirmed that cancer cells exposed to PUFAs did not enter apoptosis (Figures S6F and S6G); staurosporine was used as a control apoptosis inducer in the above experiments. By contrast, several lines of evidence indicated that PUFAs induced ferroptosis under acidic conditions. We first used the bona fide ferroptosis inducer erastin and found that it dramatically increased the cytotoxic effects of DPA and DHA in 3D tumor spheroids (from both HCT-116 and FaDu cancer cells) but did not influence the effects of PA that remained non-toxic (Figures 3E and S7A); similar effects were obtained with RSL3, another ferroptosis inducer (Figure S7B). We next examined the expression of the central regulator of ferroptosis glutathione (GSH) peroxidase-4 (GPX4) and

cells (A) and used at the concentrations of 50 μM in HCT-116 spheroids (B). Effects of 50 μM DHA or DPA on the growth of 3D tumor HCT116 spheroids cultured at the indicated pH (C) or in the presence of 22 mM bicarbonate (bicarb) (D). Representative pictures of 3D spheroids at the end of the experiment (B and C) or at day 7 (D) are presented. Scale bar, 500 μm.

(E) Detection of the acidic compartment within 3D FaDu spheroids using the acidic pH reporter pHLIP conjugated to Alexa-568 fluorophore. Scale bar, 100 μm.

(F) Detection of FA-induced cell death in the center of FaDu spheroids using PI; note the lack of response to palmitate versus DPA and DHA (96 h). Scale bar, 200 μm.

Data are represented as mean ± SEM of either $\geq$4 independent cultures (A) or 6 different spheroids (B–D). Significance was determined by two-way ANOVA with Sidak's multiple comparison test (A), one-way ANOVA with Tukey's multiple comparison test at endpoint (B–D), or Student's t test (E). *$p < 0.05$; **$p < 0.01$; ***$p < 0.001$. See also Figure S2.

Please cite this article in press as: Dierge et al., Peroxidation of n-3 and n-6 polyunsaturated fatty acids in the acidic tumor environment leads to ferroptosis-mediated anticancer effects, Cell Metabolism (2021), https://doi.org/10.1016/j.cmet.2021.05.016

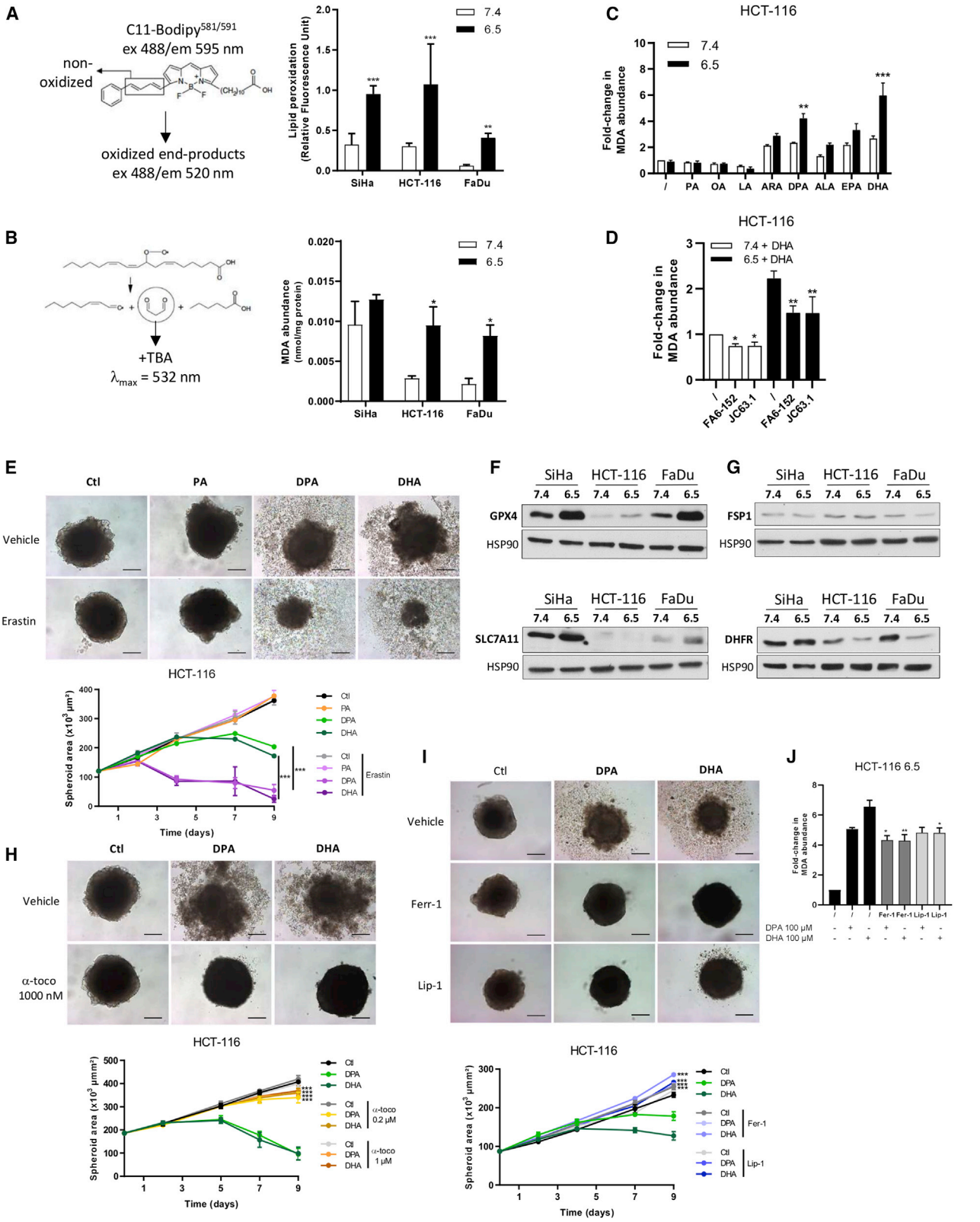

Figure 3. n-3 and n-6 PUFAs increase the extent of lipid peroxidation and promote ferroptosis under acidosis

(A and B) Detection of basal levels of peroxidation in pH 6.5-adapted and pH 7.4-cultured cancer cells using BODIPY 581/591 undecanoic acid as a peroxidation sensor (A) and by measuring the accumulation of malondialdehyde (MDA) (B).

(legend continued on next page)

Please cite this article in press as: Dierge et al., Peroxidation of n-3 and n-6 polyunsaturated fatty acids in the acidic tumor environment leads to ferroptosis-mediated anticancer effects, Cell Metabolism (2021), https://doi.org/10.1016/j.cmet.2021.05.016

found that it was significantly upregulated under acidic conditions (Figures 3F and S7C for quantification); a similar trend was observed for the cystine/glutamate transporter SLC7A11, the functional subunit of system x_c, critical to support cellular GSH biosynthesis (Figures 3F and S7C for quantification). Exposure to exogenous PUFAs did not further upregulate GPX4 and SLC7A11 (Figures S7D and S7E), suggesting that the observed alterations result from an intrinsic extent of oxidative stress in 6.5/cancer cells. While no significant changes in acyl-CoA synthetase LC family member 4 (ASCL4) expression could be observed (Figure S7F), different extents of reduction in other key players in ferroptosis, namely dihydrofolate reductase (DHFR) and ferroptosis suppressor protein-1 (FSP-1), were observed in 6.5/cancer cells (Figures 3G and S7G for quantification), supporting an increased susceptibility to ferroptosis arising from a deficit in radical trapping systems. To more firmly establish the preferred induction of ferroptosis in 6.5/cancer cells, we used lipophilic antioxidant alpha-tocopherol (vitamin E) (Figure 3H) as well as ferroptosis inhibitors ferrostatin-1 and liproxstatin-1 (Figures 3I and S8A) and documented that they could prevent cell death and associated spheroid disaggregation in response to DPA or DHA. Moreover, we quantified the levels of MDA upon exposure to ferrostatin-1 and liproxstatin-1 and found that both significantly reduced the extent of MDA generation resulting from DPA and DHA exposure (Figures 3J and S7B).

DGAT inhibitors prevent the formation of lipid droplets and alter the cellular fate of PUFAs

Our finding that PUFAs preferentially induced ferroptotic cell death under acidosis in proportion to the number of double bonds suggested that LDs might represent a strategy to divert the excess of captured PUFAs from lipid peroxidation. While a direct stoichiometric relationship exists between the number of unsaturations and the amounts of reactive aldehydes that can be generated, we also examined the possibility of a differential metabolic degradation of PUFAs. We therefore measured the oxygen consumption rate (OCR) in response to different FAs and found that oxidative metabolism of PUFAs in 6.5/cancer cells was significantly reduced in proportion to the number of double bonds (Figure 4A); a similar reduction in OCR was obtained when mixtures of SFAs (i.e., palmitate) and PUFAs were used (Figure 4B). Altogether these data strongly suggest that an increased availability of PUFAs (less efficiently degraded in proportion of the number of double bonds) may account for their preferred LD storage but also increased propensity to undergo peroxidation.

We next reasoned that preventing PUFA storage into LDs could enhance the deleterious effects of lipid peroxidation in the tumor acidic compartment. For this purpose, we used inhibitors of diacylglycerol acyltransferases (DGAT1 and DGAT2), which are responsible for the formation of triglycerides from diacylglycerol and acyl-CoA. We found that DGAT1 inhibitor (DGAT1i) was more efficient to prevent LD formation in 6.5/cancer cells than DGAT2 inhibitor (DGAT2i) (Figures 4C, 4D, S9A, and S9D). GC-FID analysis of the cellular fate of DHA in the presence of DGAT1i confirmed that the amount of DHA found in the NL fraction was reduced while it was significantly increased in the FFA and PL fractions (Figure 4E, top panels). While palmitate accumulation as NL was also reduced, no significant changes in the FFA and PL fractions were observed (Figure 4E, bottom panels). Finally, we measured the levels of MDA to further prove the increased potential of ferroptosis induction upon DGAT inhibition. While DGAT1i barely influenced the generation of MDA in the presence of palmitate, it strongly increased DHA-induced MDA generation in 6.5/cancer cells (Figure 4F).

DGAT inhibitors enhance the acidosis-triggered cytotoxic effects of PUFAs

We next evaluated the effects of DGAT inhibitors on the extent of PUFA-induced cytotoxicity. We found that DGAT1i increased the cytotoxic effects of DPA and DHA (to a larger extent than DGAT2i) in acid-adapted cancer cells, while they had no impact on the viability of corresponding 7.4/cancer cells (Figures 5A, S10A, and S10B). By contrast, either drug did not influence the effect of palmitate in 6.5/cancer cells (Figures 5A, S10A, and S10B). We next examined the effects of DGAT inhibition in 3D HCT-116 and FaDu tumor spheroid models. We found that DGAT1i and DGAT2i both increased the growth inhibitory effects of DPA and DHA (Figures 5B and S10C), while they did not influence the effects resulting from PA exposure (Figures 5B and S10C; quantification in Figures S10D and S10E). Interestingly, combination of both DGAT1i and DGAT2i led to more profound effects than single treatment (Figures 5B and S10C). To further prove the enhancing potential of DGATi on PUFA cytotoxic effects in acidic cancer cells, we examined whether PUFA dosage could be reduced when combined with DGATi. We found that a concentration of DPA or DHA as low as 10 μM was actually already leading to cytotoxic effects in 3D HCT-116 spheroids when combined with DGAT1i (Figure 5C). Using a lentiviral CRISPR-Cas9 approach, we documented that DGAT1 genetic silencing also significantly increased the cytotoxic effects of DHA and DPA on 3D tumor spheroids (Figures S10F and

(C) Effects of a 24-h exposure to the indicated FA (see Figure 1 legend for abbreviations) on MDA accumulation in pH 6.5-adapted and pH 7.4-cultured HCT-116 cancer cells.
(D) Effects of a 24-h treatment with two CD36-blocking antibodies (FA6-152 and JC63.1) on the extent of DHA-induced MDA accumulation in HCT-116 cancer cells.
(E) Effects of ferroptosis inducer erastin on the growth of 3D HCT-116 tumor spheroids in the presence (or not) of 50 μM PA, DPA, and DHA for increasing periods of time; representative pictures of spheroids at day 9 are also shown. Scale bar, 500 μm.
(F and G) Representative immunoblots for GPX4 and SLC7A11 (F) and FSP-1 and DHFR (G) in the indicated cancer cells.
(H and I) Effects of 1 μM alpha-tocopherol (vitamin E) (H) and ferrostatin-1 and liproxstatin-1 (I) on 3D HCT-116 spheroids exposed to 50 μM DPA or DHA for increasing periods of time; representative pictures of spheroids at day 9 are also shown. Scale bar, 500 μm.
(J) Effects of ferrostatin-1 (Fer-1) and liproxstatin-1 (Lip-1) on MDA accumulation in HCT-116 cancer cells exposed to 100 μM DPA or DHA.
Data are represented as mean ± SEM of ≥3 independent experiments (A–D and J) or 6 different spheroids (E, H, and I). Significance was determined by two-way ANOVA with Sidak's multiple comparison test (A–C), one-way ANOVA with Tukey's multiple comparison test at endpoint (E, H, and J), or Student's t test (D). *$p < 0.05$; **$p < 0.01$; ***$p < 0.001$. See also Figure S3.

Please cite this article in press as: Dierge et al., Peroxidation of n-3 and n-6 polyunsaturated fatty acids in the acidic tumor environment leads to ferroptosis-mediated anticancer effects, Cell Metabolism (2021), https://doi.org/10.1016/j.cmet.2021.05.016

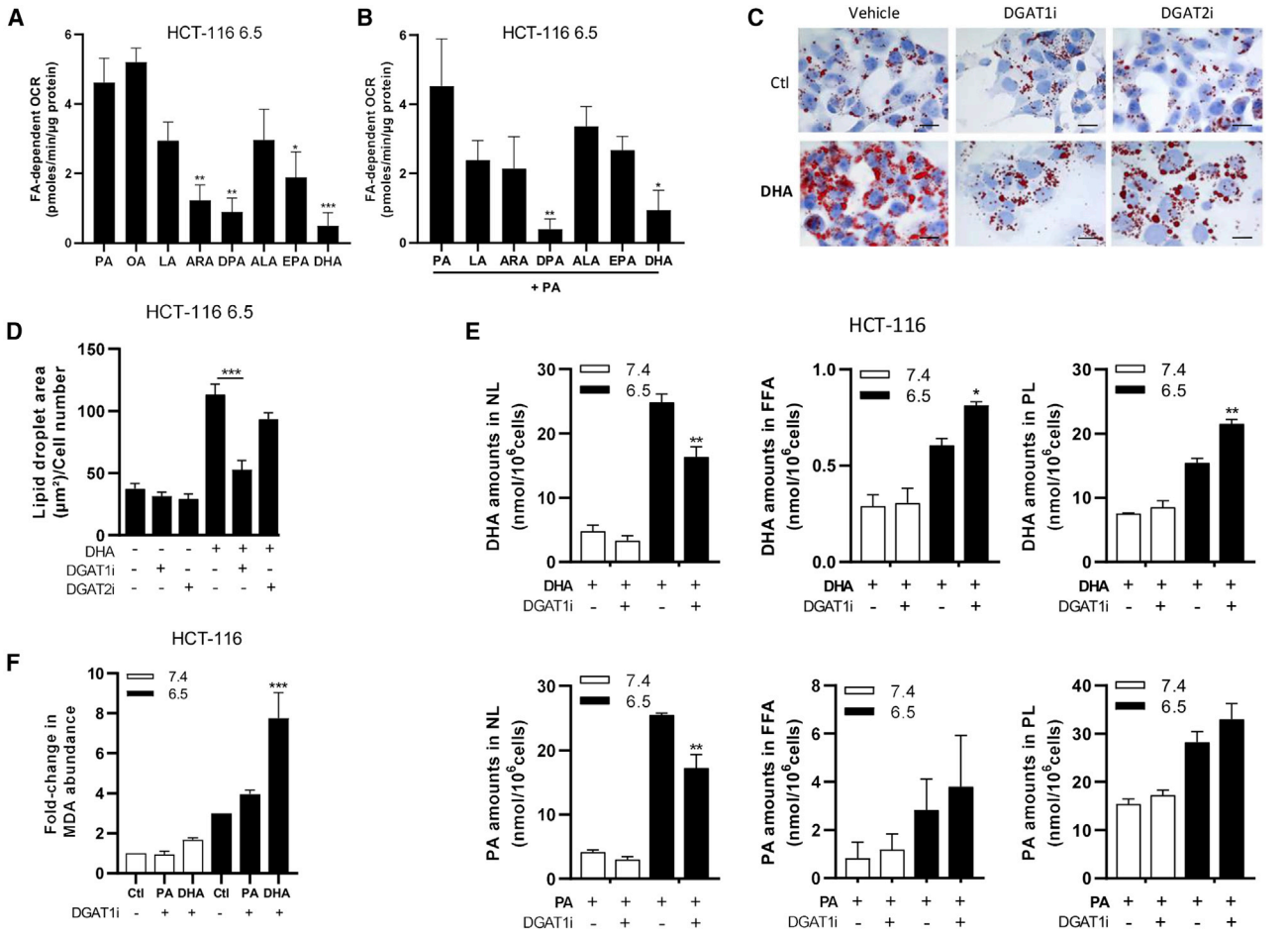

Figure 4. DGAT inhibition reduces PUFA accumulation as triglycerides in LDs and promotes lipid peroxidation

(A and B) Effects of the indicated FA (100 μM) (A) or the mixture of the indicated FA (50 μM) combined with 50 μM palmitate (PA) (B) on the OCR in pH 6.5-adapted cancer cells.

(C and D) Representative pictures (C) and quantification (D) of ORO-stained LDs in pH 6.5-adapted HCT-116 cancer cells upon 24-h exposure to 50 μM DHA and either 15 μM A922500 (DGAT1i) or 10 μM PF06424439 (DGAT2i). Scale bar, 20 μm.

(E) DHA (top) and PA (bottom) abundance in NL, FFA, and PL fractions isolated from 6.5/ and 7.4/HCT-116 cells upon 24-h exposure to 50 μM DHA or PA and DGAT1 inhibitor.

(F) Effect of DGAT1 inhibitor on MDA accumulation in HCT-116 cancer cells exposed for 24 h to 100 μM palmitate (PA) or DHA.

Data are represented as mean ± SEM of ≥3 independent experiments (A, B, D, and F). Significance was determined by one-way ANOVA with Tukey's multiple comparison test (A, B, and D), two-way ANOVA with Sidak's multiple comparison test (E), or Student's t test (F) *p < 0.05; **p < 0.01; ***p < 0.001. See also Figure S4.

S10G). Finally, to prove that the sensitizing effects of DGATi were related to enhanced ferroptosis, we repeated the above experiments in the presence of ferrostatin-1 and liproxstatin-1. Both ferroptosis inhibitors prevented the cytotoxic effects of DHA and DPA in 3D HCT-116 and FaDu tumor spheroids (Figures 5D and S11A). Altogether, these results indicate that preventing PUFA buffering into LDs with DGATi represents an achievable strategy to selectively promote ferroptotic death of acidic cancer cells upon exposure to minimal amounts of PUFAs.

Mouse tumor growth is inhibited in response to n-3 LC-PUFA-based diet and further delayed when combined with DGATi or ferroptosis inducer

To further evaluate the effects of PUFAs *in vivo*, we fed mice either olive oil- or concentrated fish oil-based isocaloric diets (Tables S1 and S2). We first showed that 4-week fish oil-based DHA-rich diet led to a highly significant n-3 PUFA enrichment in circulating lipids (as FFA, PL, and NL) (versus mice fed on the olive oil-based OA-rich diet) (Figure 6A). Moreover, the total amounts of FAs in the serum were reduced by 68% and 47% in the FFA and NL fractions of mice fed on the DHA-rich diet, respectively (Figure 6B). We also measured FA accumulation in the mouse liver and found a similar distribution with a net enrichment in the n-3 PUFA pool in mice fed on the concentrated fish oil-rich diet at the expense of MUFAs that amounted to 23% of total FAs (versus 72% in mice fed on OA-rich diet) in the liver NL fraction (Figures S12A and S12B).

A clear difference in the evolution of mouse weights was observed between the two diets. A significant reduction in weight was observed at the initiation of the treatment with the

Please cite this article in press as: Dierge et al., Peroxidation of n-3 and n-6 polyunsaturated fatty acids in the acidic tumor environment leads to ferroptosis-mediated anticancer effects, Cell Metabolism (2021), https://doi.org/10.1016/j.cmet.2021.05.016

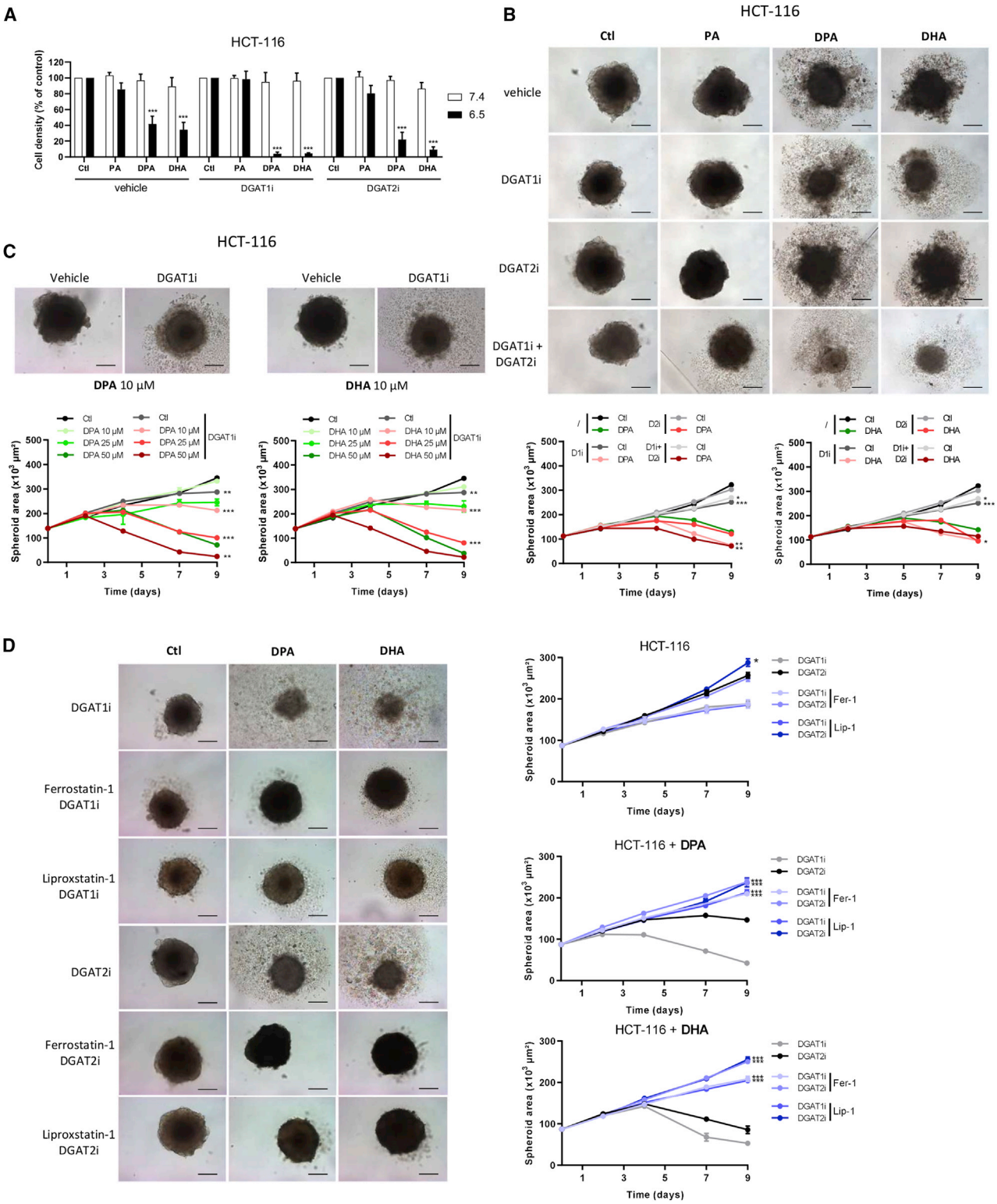

Figure 5. DGAT inhibitors enhance acidosis-triggered cytotoxic effects of n-6 and n-3 LC-PUFAs

(A and B) Effects of DGAT inhibitors (15 μM A922500 [DGAT1i] or 10 μM PF06424439 [DGAT2i]) on the growth of pH 6.5-adapted and pH 7.4-cultured HCT-116 cancer cells (A), as well as on the growth of 3D tumor HCT116 spheroids (B). Cells were treated for 72 h (A) or for increasing periods of time (B) in the presence of 50 μM PA, DPA, or DHA; representative pictures of spheroids were taken at day 9. Scale bar, 500 μm.

(C) Titration of the effects of DPA and DHA on the growth of 3D tumor HCT-116 spheroids in the presence of DGAT1 inhibitor; representative pictures of spheroids were taken at day 9. Scale bar, 500 μm.

(legend continued on next page)

Please cite this article in press as: Dierge et al., Peroxidation of n-3 and n-6 polyunsaturated fatty acids in the acidic tumor environment leads to ferroptosis-mediated anticancer effects, Cell Metabolism (2021), https://doi.org/10.1016/j.cmet.2021.05.016

DHA-rich diet (Figure 6C). Weight gain then remained constantly reduced (0.14 g per day versus 0.06 g per day for the OA-rich diet) (Figure 6C) and was not associated with a reduction in food consumption that was constant regardless of the diet (around 3 g per day), except on the first day of diet initiation (Figure 6D). Treatment with DGATi did not influence weight gain and food consumption in either diet group (Figures 6C and 6D), and similar results were obtained in mice not bearing tumors (data not shown). To identify the origin of the weight loss, we carefully dissected subcutaneous and visceral fat tissues and found that while white adipose tissue (WAT) was reduced by almost 50% in mice fed on DHA-rich diet (Figure 6E), brown adipose tissue (BAT) was not altered and even slightly more abundant in these mice (versus mice fed on OA-rich diet) (Figure 6F). As a result, the adiposity index was significantly reduced in response to DHA-rich diet (Figure 6G). Analysis of FA subtype distribution in WAT further indicated that the major differences were a significant n-3 PUFA accumulation in mice fed on DHA-rich diet together with a lesser proportion of MUFAs in the NL fraction (versus OA-rich diet) (Figures S12C and S12D). Of note, we also measured serum LPS as a reflection of metabolic endotoxemia and did not find significant differences between mice fed OA-rich or DHA-rich diet (Figure S13A).

Mice were injected with HCT-116 cancer cells 2 weeks after initiation of either diet, i.e., at a time when mice of both groups were consuming the same daily amounts of food. The development of acidosis in these tumors was verified using a pHLIP peptide as an *in vivo* acid sensor. A highly specific accumulation of Alexa647-conjugated pHLIP peptide could be detected, whereas a control pH-insensitive peptide (K-pHLIP conjugated to Alexa568) failed to label tumors (Figure S13B). A significant tumor growth delay was observed in mice fed the DHA-rich diet (versus OA-rich diet) (Figure 6H), together with a significant prolongation of mouse survival (Figures 6I and S13C). Importantly, while the DHA-rich diet per se very significantly delayed tumor growth, DGAT1i further delayed tumor growth in mice fed the DHA-rich diet, but not the OA-rich diet (Figures 6H and 6I). GC-FID measurements of FA accumulated into tumors confirmed a net increase in n-3 PUFAs as FFAs, PL, and NL for the mice fed the DHA-rich diet (versus OA-rich diet) (Figure 6J). Of note, in the tumors of mice fed the OA-rich diet, most n-6 PUFAs consisted in LA (C18:2) that is much less peroxidable than n-3 EPA (C20:5) and DHA (C22:6), the two most enriched PUFAs in the tumors of mice fed the fish oil-based diet (Figure S13D). This was confirmed by immunodetection of MDA but also 4-hydroxy-2E-hexenal (4-HHE), the most prominent by-product of hydroperoxy derivatives of n-3 PUFAs. Indeed, we found increased levels of peroxidation in the tumors of mice fed the DHA-rich diet (versus OA-rich diet) (Figure 6K) (1.7-fold increase for MDA, $p < 0.01$, $n = 5–6$; 2.5-fold increase for 4-HHE, $p < 0.001$, $n = 5–7$). We did not observe signs of systemic toxicity as determined by analyzing circulating hepatic enzymes (ALT and AST) and blood urea nitrogen (BUN) that remained in the physiological ranges (Figures S13E–S13G); serum MDA was also unaltered by either diet or by the DGATi treatment (Figure S13H).

Finally, we treated HCT-116 tumor-bearing mice fed the DHA-rich diet either with ferroptosis-inducing or -inhibiting agents (Figures 6L–6N). We found that the DHA-rich diet increased the antitumor effects of sulfasalazine, a cost-effective ferroptosis inducer (Lang et al., 2019) (Figures 6L and 6M), without any influence on mouse weight (Figure S13I); erastin was also used as another ferroptosis inducer and similarly accentuated the effects of the DHA-rich diet on tumor growth (Figures S13J–S13L), though to a smaller extent probably related to the metabolic instability of this compound (Zhang et al., 2019). More importantly, administration of the ferroptosis inhibitor ferrostatin-1 stimulated tumor growth and significantly reduced the survival of mice fed the DHA-rich diet (Figures 6L and 6N), confirming a role of ferroptosis in the capacity of n-3 PUFA-rich diet to delay tumor growth.

DISCUSSION

How diet impacts cancer outcomes is of great interest to patients (Zick et al., 2018), but today few clinical trials have addressed how dietary factors affect cancer progression (Lévesque et al., 2019). Yet the re-emergence of tumor metabolism as a promising field of investigation for the identification of innovative anticancer treatments offers today an opportunity to further explore the link between nutrition and tumor growth and optimize clinical protocols. In this work, we examined the beneficial role of PUFAs in the fight against cancer through a specific angle. Indeed, while numerous recent contributions have validated lipid metabolism as a key target to be inhibited in tumors (Butler et al., 2020; Corbet and Feron, 2017; Snaebjornsson et al., 2020), we document here that one can instead exploit the preferred FA metabolism within the acidic tumor compartment to introduce deleterious FAs, in particular LC-PUFAs. Our previous demonstration that acidic cancer cells accumulated LDs under acidosis (Corbet et al., 2020) led us to consider that excess FA uptake could also represent a vulnerability factor above a given threshold. We actually found that accumulation of n-3 LC-PUFAs but also n-6 LC-PUFAs is toxic for acid-adapted cancer cells as well as in 3D spheroids recapitulating the spontaneous formation of H^+ gradients within tumors. Mechanistically, we provide evidence that ferroptosis, an iron-dependent, non-apoptotic form of cell death associated with oxidized lipids, is promoted when acidic cancer cells fail to buffer the enhanced uptake of PUFAs and expose themselves to the detrimental effects of peroxidation. First, the cytotoxic effects were observed in response to PUFAs, but not MUFAs or SFAs, and were associated with a CD36-dependent increase in MDA generation. Second, the antitumor effects were observed with both the n-6 and n-3 PUFA series in direct proportion to the number of double bonds, supporting an intrinsic chemical effect

(D) Effects of ferrostatin-1 (Fer-1) and liproxstatin-1 (Lip-1) on 3D HCT-116 spheroids exposed to DGAT inhibitors and either 50 μM DPA or DHA for increasing periods of time; representative pictures of spheroids at day 9 are also shown. Scale bar, 500 μm.

Data are represented as mean ± SEM of 3 independent experiments (A) or as mean ± SEM of 6 different spheroids (B–D). Significance for the effects of DGATi (versus corresponding vehicle) was determined by two-way ANOVA with Sidak's multiple comparison (A) or one-way ANOVA with Tukey's multiple comparison test at endpoint (B–D). *$p < 0.05$; **$p < 0.01$; ***$p < 0.001$. See also Figure S5.

Please cite this article in press as: Dierge et al., Peroxidation of n-3 and n-6 polyunsaturated fatty acids in the acidic tumor environment leads to ferroptosis-mediated anticancer effects, Cell Metabolism (2021), https://doi.org/10.1016/j.cmet.2021.05.016

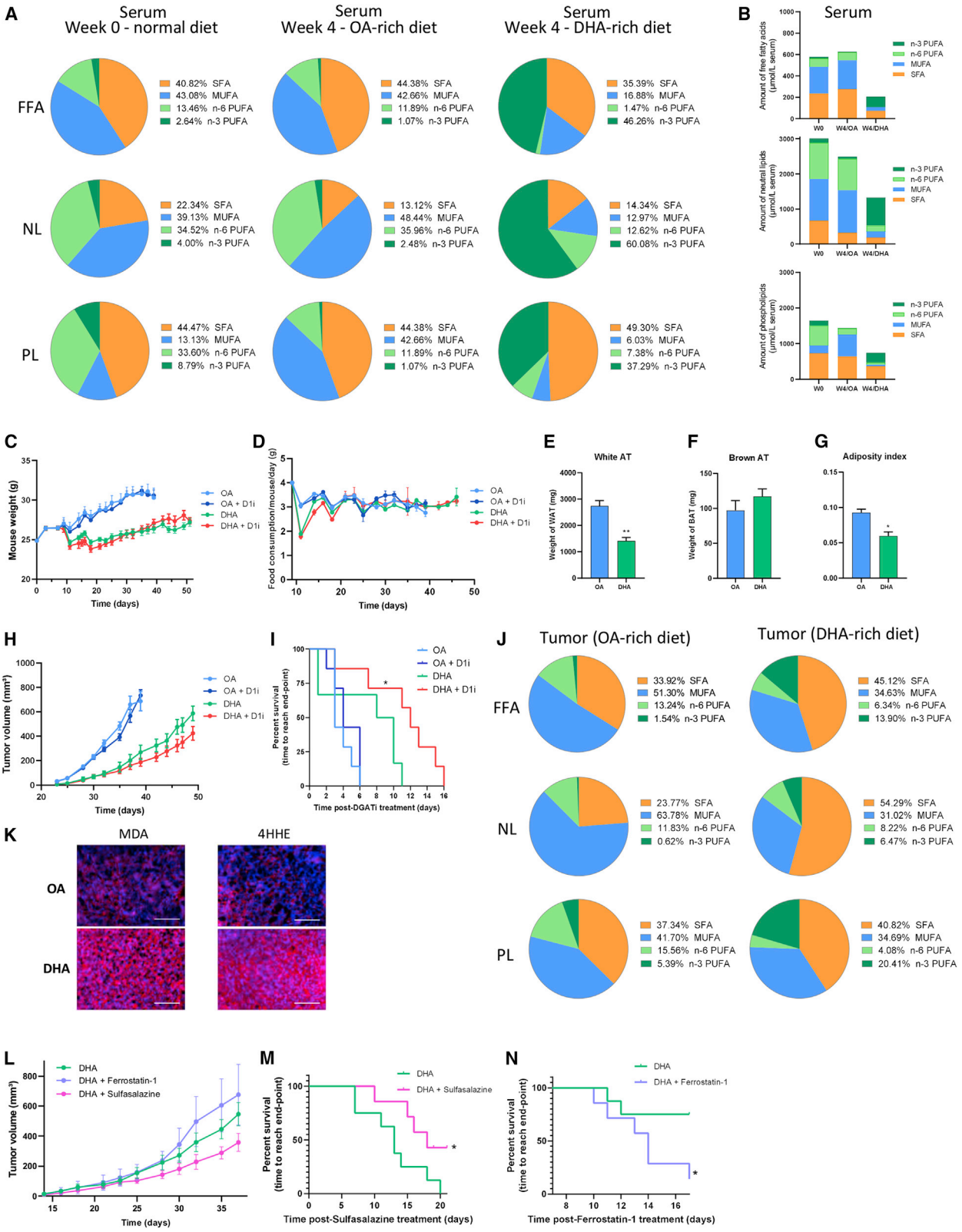

Figure 6. n-3 LC-PUFA-rich diet delays tumor growth in mice in a ferroptosis-dependent manner

(A and B) Repartition (A) and amounts (B) of SFAs, MUFAs, and n-6 and n-3 PUFAs in blood before (week 0 or W0) and after 4 weeks of either OA- or DHA-rich isocaloric diets (W4/OA and W4/DHA, respectively).

(legend continued on next page)

instead of an alteration in signaling pathways driven by PUFA metabolites (i.e., eicosanoids). Third, LC-PUFA-dependent cell death in 3D spheroids was fully reversible upon exposure to various radical trapping agents and, conversely, further enhanced in response to the ferroptosis inducer erastin. Fourth, peroxidation byproducts MDA and 4-HHE were significantly increased in tumors of mice fed a DHA-rich diet and, while ferroptosis inhibitor ferrostatin-1 reduced the tumor growth inhibitory effects of the DHA-rich diet, the ferroptosis inducer sulfasalazine further enhanced the anticancer effects of that diet.

Alteration in membrane integrity resulting from a decrease in the proportion of PUFAs within lipid bilayers (and thus of their kinked tails that prevent adjacent phospholipids from packing) is very often proposed to account for ferroptotic cell death downstream of lipid peroxidation. Our experiments indicate that ferroptosis induction in response to ambient tumor acidosis may also contribute to anticancer effects through deleterious cross-linking of various cellular components with toxic aldehydes such as 4-hydroxy-2E-hexenal (4-HHE) or malondialdehyde (MDA) derived from the decomposition of lipid hydroperoxides. Lately, regardless of the description of ferroptosis as a type of cell death that occurs through excessive peroxidation of PUFAs, few studies related to ferroptosis have focused on the therapeutic potential of LC-PUFAs. Instead, many authors have examined the nature of the genes involved in the induction and execution of this iron-catalyzed form of necrosis (Hassannia et al., 2019). Also, confusion about the interest of LC-PUFA dietary supplementation has arisen from the lack of beneficial effects of n-3 PUFAs on cancer incidence as reported in systematic review and meta-analysis of randomized trials (Hanson et al., 2020). Still, recent findings suggest that the promotion of ferroptosis by PUFAs could be particularly suited to kill a subset of cancer cell populations with acquired or intrinsic resistance to treatments and/or a high capacity for invasion. Therapy-resistant mesenchymal cancer cells were, for instance, documented to be highly dependent on a lipid-peroxidase pathway that protects against ferroptosis, ZEB1 acting as the molecular link between epithelial-mesenchymal transition, and associated increase in FA uptake and lipid peroxide-associated vulnerability (Shimada et al., 2016; Viswanathan et al., 2017). Interestingly, we recently reported that tumor acidosis fosters autocrine ZEB-1/TGF-beta2 signaling, which in turn drives lipid droplet accumulation and rewires lipid metabolism to fulfill cellular energy needs during metastatic spreading (Corbet et al., 2020). These observations may be further related to the recent report by Ubellacker and colleagues who documented that cancer cells that metastasize through lymph resist ferroptosis by reducing oxidative stress (Ubellacker et al., 2020). Altogether, these data suggest that while PUFAs may not exert global antitumor effects, the high tropism of acidic, drug-resistant, and/or pro-invasive cancer cells for FAs accounts for specific deleterious effects of LC-PUFAs toward tumor cells directly participating to disease progression. Indirectly, this specificity toward acidic tumor tissues (versus other tumor compartments but also healthy tissues at neutral pH) supports dietary LC-PUFA administration as a safe and selective intervention with a favorable risk-benefit balance.

Importantly, our work also provides evidence that the needed amounts of bioactive n-3 LC-PUFAs in the tumor may be reduced by taking advantage of the co-administration of DGAT inhibitors. Blocking the esterification of fatty acyl-CoA with diacylglycerol prevents the formation of triglycerides but also modifies the fate of acyl-CoA that accumulates in the cytosol and incorporates into plasma membranes (Figure 4E). Remarkably, in 3D tumor spheroids and *in vivo*, we showed that DGAT inhibition induces significant cytotoxic effects when combined with LC-PUFAs, but not with SFAs or MUFAs. Our findings position DGATi administration and dietary n-3 LC-PUFAs as a highly relevant therapeutic combination, the former making the latter more prone to undergo peroxidation and induce ferroptosis. DGAT1i appears to be more potent than DGAT2i, in agreement with evidence that DGAT1 is more important in protecting the ER from lipotoxic effects of excess "exogenous" FAs, while DGAT2 has a more ancient function for mediating TG synthesis of *de novo*-synthesized FAs (Chitraju et al., 2017; Yen et al., 2008). These data actually expand on the antitumor potential of DGATi. For instance, DGAT1 inhibition was recently reported to drive FA-dependent mitochondrial over boost in glioblastoma, leading to apoptosis and significant growth inhibitory effects (Cheng et al., 2020). In our study, DGAT inhibition did not lead to tumor growth inhibition in mice fed on OA-rich diet but did in mice fed on DHA-rich diet, indicating that differences may exist between cancer types and/or according to the drug dosages and exposure times. More generally, our data underline the potential of pharmacological approaches able to increase intracellular PUFA availability by other means than blocking their incorporation into TGs. Interestingly, Perez and colleagues reported that an inhibitor of ether lipid-generating enzyme alkyl-glycerone phosphate synthase (AGPS) could sensitize cells to the toxic effects of dihomogamma-linolenic acid (DGLA), a n-6 PUFA known to induce sterility in *C. elegans*. In the latter study, germ cell death could, however, not be recapitulated by dietary LA, ALA, or

(C and D) Time course of mouse weight gain (C) and food consumption (D) in mice fed on either diet and treated (or not) with 3 mg/kg DGAT1 inhibitor A922500 (D1i).

(E–G) Extent of white (WAT) (E) and brown (BAT) (F) adipose tissue and adiposity index (G) as determined 4 weeks after the initiation of either diet.

(H and I) Tumor growth (H) and corresponding Kaplan-Meier survival curves (I) in mice fed with OA- or DHA-rich diets and treated (or not) with DGAT1 inhibitor.

(J) Repartition of SFAs, MUFAs, and n-6 and n-3 PUFAs in the tumors of mice fed with either diet.

(K) Representative pictures of MDA and 4-HHE immunostaining in tumors collected from OA- and DHA-rich diets; fold changes are mentioned in the text. Scale bar, 100 μm.

(L–N) Tumor growth (L) and corresponding Kaplan-Meier survival curves in mice fed with DHA-rich diet and treated (or not) with sulfasalazine (M) or ferrostatin-1 (N).

Data are represented as mean of blood dosages for 3 mice fed on DHA-rich diet for 4 weeks versus mice on normal diet (week 0) or fed on OA-rich diet for 4 weeks (A and B), as mean ± SEM of 6 to 8 mice (C–I and K–N) per condition or as mean of tumor dosages for mice (n = 4) fed the indicated diet (J). Significance was determined by Student's t test (E–G) or log-rank (Mantel-Cox) test (I, M, and N). *$p < 0.05$; ***$p < 0.001$. See also Figure S6 and Tables S1 and S2.

EPA, suggesting selective structure-specific peroxidation by cytochrome P450 or lipoxygenase enzymes. A deficiency in DECR1, a critical enzyme in the PUFA beta-oxidation pathways, was also associated with enhanced mitochondrial oxidative stress and higher potential of lipid peroxidation (Nassar et al., 2020). Further studies are warranted to determine whether the intrinsic pharmacological effects of drugs used to influence the impact of dietary PUFA supplementation will offer additional beneficial effects or will instead potentially induce toxicity in organs where FAs are used as major nutrients such as the heart.

In conclusion, the shared effects of n-3 and n-6 LC-PUFAs on acidic cancer cells (versus preferred resolution of the inflammatory cycle by n-3, but not n-6 eicosanoids) underpin a major contribution of lipid peroxidation in anticancer effects of LC-PUFAs. Our study positions the rewiring of lipid metabolism associated with tumor acidosis not as a druggable target to inhibit but as a cancer cell vulnerability that can be exploited to locally increase LC-PUFA effects. The well-established link between tumor acidosis and disease progression, including through increased invasiveness, drug resistance, and immune escape, makes dietary n-3 LC-PUFA supplementation a particularly relevant strategy to be implemented.

Limitations of study

This study describes the anticancer effects resulting from excess LC-PUFA accumulation in cancer cells cultured under acidosis, in 3D tumor spheroids as well as in mouse tumors. This brings the question of the concentration of bioactive n-3 LC-PUFAs that can be reached in humans. In our experiments, we paid attention to work in the presence of serum so that exogenous PUFAs were not the only FAs in media but were actually mixed with serum-containing FAs. Significant cell death was observed with concentrations of n-6 DPA and n-3 DHA as low as 10 μM (i.e., ~10% of total FAs present in the medium). As a reference, we recently performed a pilot study in human volunteers (data not shown), which indicates that the daily consumption of 4.8 g concentrated fish oil (containing 80% n-3 LC-PUFA) for 1 week allowed them to reach total plasma n-3 LC-PUFA content around ~500 μM. Further investigation is warranted to examine the bioavailability of n-3 LC-PUFAs in cancer patients upon dietary supplementation, including after longer diet periods than what was possible in our study with short-lived tumor-bearing mice. Of interest, the reduction in adiposity index observed in our mouse experiments and reported elsewhere (Lund et al., 2018) in response to marine n-3 PUFA-rich diet was associated with a reduced proportion of MUFAs in blood, adipose tissue, and liver. Additional work is required to determine whether such systemic effects of n-3 LC-PUFAs may also indirectly contribute to tumor growth inhibitory effects through a reduction in the proportion of bioavailable MUFAs. Also, a careful evaluation of the contribution to our *in vivo* findings of the PUFA effects on the microbiota is needed. Finally, while DGAT inhibitors as used in this study are reaching the clinic, a flag of attention needs to be raised about the *in vivo* stability of ferroptosis modulators as recently emphasized by Jiang and colleagues (Jiang et al., 2021).

STAR★METHODS

Detailed methods are provided in the online version of this paper and include the following:

- KEY RESOURCES TABLE
- RESOURCE AVAILABILITY
  - Lead contact
  - Materials availability
  - Data and code availability
- EXPERIMENTAL MODEL AND SUBJECT DETAILS
  - Cell lines & culture
  - Mouse strains
- METHOD DETAILS
  - 2D culture treatment
  - Oil red O staining
  - Fatty acid quantification
  - 3D spheroid models
  - MDA measurements
  - Peroxidation potential
  - Flow cytometry
  - Western blot
  - Oxygen-consumption rate measurements
  - *In vivo* mouse experiment
- QUANTIFICATION AND STATISTICAL ANALYSIS

SUPPLEMENTAL INFORMATION

Supplemental information can be found online at https://doi.org/10.1016/j.cmet.2021.05.016.

ACKNOWLEDGMENTS

This work was supported by grants from the Fonds de la Recherche Scientifique (F.R.S. – FNRS), the Televie, the (Belgian) Foundation against Cancer, the J. Maisin Foundation, the Fondation Louvain, and an Action de Recherche Concertée (ARC 19/24-096). E. Dierge and E.B. are Télévie PhD and postdoctoral fellows, respectively. C.C. is an F.R.S. – FNRS Research Associate and C.D. is a senior F.R.S. – FNRS Research Associate.

AUTHOR CONTRIBUTIONS

Conceptualization, E. Dierge, Y.L., and O.F.; experimental work, E. Dierge, E. Debock, C.G., E.M., and L.M.; data analysis and interpretation, E. Dierge, Y.L., and O.F.; methodology, E. Dierge, E.B., and C.C.; writing – review & editing, E. Dierge, C.C., C.D., Y.L., and O.F.; funding and resources, C.D., Y.L., and O.F.; supervision, Y.L. and O.F.

DECLARATION OF INTERESTS

The authors declare no competing interests.

Received: November 30, 2020
Revised: April 6, 2021
Accepted: May 17, 2021
Published: June 11, 2021

REFERENCES

Bagchi, D.P., and MacDougald, O.A. (2019). Identification and dissection of diverse mouse adipose depots. J. Vis. Exp. *149*. https://doi.org/10.3791/59499.

Berquin, I.M., Edwards, I.J., and Chen, Y.Q. (2008). Multi-targeted therapy of cancer by omega-3 fatty acids. Cancer Lett *269*, 363–377.

Bligh, E.G., and Dyer, W.J. (1959). A rapid method of total lipid extraction and purification. Can. J. Biochem. Physiol. *37*, 911–917.

Butler, L.M., Perone, Y., Dehairs, J., Lupien, L.E., de Laat, V., Talebi, A., Loda, M., Kinlaw, W.B., and Swinnen, J.V. (2020). Lipids and cancer: emerging roles in pathogenesis, diagnosis and therapeutic intervention. Adv. Drug Deliv. Rev. *159*, 245–293.

Cheng, X., Geng, F., Pan, M., Wu, X., Zhong, Y., Wang, C., Tian, Z., Cheng, C., Zhang, R., Puduvalli, V., et al. (2020). Targeting DGAT1 ameliorates glioblastoma by increasing fat catabolism and oxidative stress. Cell Metab *32*, 229–242.e8.

Chitraju, C., Mejhert, N., Haas, J.T., Diaz-Ramirez, L.G., Grueter, C.A., Imbriglio, J.E., Pinto, S., Koliwad, S.K., Walther, T.C., and Farese, R.V., Jr. (2017). Triglyceride synthesis by DGAT1 protects adipocytes from lipid-induced ER stress during lipolysis. Cell Metab *26*, 407–418.e3.

Corbet, C., and Feron, O. (2017). Emerging roles of lipid metabolism in cancer progression. Curr. Opin. Clin. Nutr. Metab. Care *20*, 254–260.

Corbet, C., Draoui, N., Polet, F., Pinto, A., Drozak, X., Riant, O., and Feron, O. (2014). The SIRT1/HIF2alpha axis drives reductive glutamine metabolism under chronic acidosis and alters tumor response to therapy. Cancer Res *74*, 5507–5519.

Corbet, C., Pinto, A., Martherus, R., Santiago de Jesus, J.P., Polet, F., and Feron, O. (2016). Acidosis drives the reprogramming of fatty acid metabolism in cancer cells through changes in mitochondrial and histone acetylation. Cell Metab *24*, 311–323.

Corbet, C., Bastien, E., Santiago de Jesus, J.P., Dierge, E., Martherus, R., Vander Linden, C., Doix, B., Degavre, C., Guilbaud, C., Petit, L., et al. (2020). TGFbeta2-induced formation of lipid droplets supports acidosis-driven EMT and the metastatic spreading of cancer cells. Nat. Commun. *11*, 454.

Davidson, S.M., Papagiannakopoulos, T., Olenchock, B.A., Heyman, J.E., Keibler, M.A., Luengo, A., Bauer, M.R., Jha, A.K., O'Brien, J.P., Pierce, K.A., et al. (2016). Environment impacts the metabolic dependencies of Ras-driven non-small cell lung cancer. Cell Metab *23*, 517–528.

D'Eliseo, D., and Velotti, F. (2016). Omega-3 fatty acids and cancer cell cytotoxicity: implications for multi-targeted cancer therapy. J. Clin. Med. *5*, 15.

DeNicola, G.M., and Cantley, L.C. (2015). Cancer's fuel choice: new flavors for a picky eater. Mol. Cell *60*, 514–523.

Dierge, E., and Feron, O. (2019). Dealing with saturated and unsaturated fatty acid metabolism for anticancer therapy. Curr. Opin. Clin. Nutr. Metab. Care *22*, 427–433.

Dierge, E., Larondelle, Y., and Feron, O. (2020). Cancer diets for cancer patients: lessons from mouse studies and new insights from the study of fatty acid metabolism in tumors. Biochimie *178*, 56–68.

Gonzalez, P.S., O'Prey, J., Cardaci, S., Barthet, V.J.A., Sakamaki, J.I., Beaumatin, F., Roseweir, A., Gay, D.M., Mackay, G., Malviya, G., et al. (2018). Mannose impairs tumour growth and enhances chemotherapy. Nature *563*, 719–723.

Hanson, S., Thorpe, G., Winstanley, L., Abdelhamid, A.S., and Hooper, L.; PUFAH group (2020). Omega-3, omega-6 and total dietary polyunsaturated fat on cancer incidence: systematic review and meta-analysis of randomised trials. Br. J. Cancer *122*, 1260–1270.

Hassannia, B., Vandenabeele, P., and Vanden Berghe, T. (2019). Targeting ferroptosis to iron out cancer. Cancer Cell *35*, 830–849.

Hopkins, B.D., Pauli, C., Du, X., Wang, D.G., Li, X., Wu, D., Amadiume, S.C., Goncalves, M.D., Hodakoski, C., Lundquist, M.R., et al. (2018). Suppression of insulin feedback enhances the efficacy of PI3K inhibitors. Nature *560*, 499–503.

Jiang, X., Stockwell, B.R., and Conrad, M. (2021). Ferroptosis: mechanisms, biology and role in disease. Nat. Rev. Mol. Cell Biol. *22*, 266–282.

Kanarek, N., Keys, H.R., Cantor, J.R., Lewis, C.A., Chan, S.H., Kunchok, T., Abu-Remaileh, M., Freinkman, E., Schweitzer, L.D., and Sabatini, D.M. (2018). Histidine catabolism is a major determinant of methotrexate sensitivity. Nature *559*, 632–636.

Lang, X., Green, M.D., Wang, W., Yu, J., Choi, J.E., Jiang, L., Liao, P., Zhou, J., Zhang, Q., Dow, A., et al. (2019). Radiotherapy and immunotherapy promote tumoral lipid oxidation and ferroptosis via synergistic repression of SLC7A11. Cancer Discov *9*, 1673–1685.

Lévesque, S., Pol, J.G., Ferrere, G., Galluzzi, L., Zitvogel, L., and Kroemer, G. (2019). Trial watch: dietary interventions for cancer therapy. Oncoimmunology *8*, 1591878.

Lien, E.C., and Vander Heiden, M.G. (2019). A framework for examining how diet impacts tumour metabolism. Nat. Rev. Cancer *19*, 651–661.

Luengo, A., Gui, D.Y., and Vander Heiden, M.G. (2017). Targeting metabolism for cancer therapy. Cell Chem. Biol. *24*, 1161–1180.

Lund, J., Larsen, L.H., and Lauritzen, L. (2018). Fish oil as a potential activator of brown and beige fat thermogenesis. Adipocyte *7*, 88–95.

Lv, M., Zhu, X., Wang, H., Wang, F., and Guan, W. (2014). Roles of caloric restriction, ketogenic diet and intermittent fasting during initiation, progression and metastasis of cancer in animal models: a systematic review and meta-analysis. PLoS One *9*, e115147.

Mayne, S.T., Playdon, M.C., and Rock, C.L. (2016). Diet, nutrition, and cancer: past, present and future. Nat. Rev. Clin. Oncol. *13*, 504–515.

Muir, A., Danai, L.V., and Vander Heiden, M.G. (2018). Microenvironmental regulation of cancer cell metabolism: implications for experimental design and translational studies. Dis. Model. Mech. *11*, dmm035758.

Nassar, Z.D., Mah, C.Y., Dehairs, J., Burvenich, I.J., Irani, S., Centenera, M.M., Helm, M., Shrestha, R.K., Moldovan, M., Don, A.S., et al. (2020). Human DECR1 is an androgen-repressed survival factor that regulates PUFA oxidation to protect prostate tumor cells from ferroptosis. eLife *9*, e54166.

Nestle, M. (2018). Perspective: challenges and controversial issues in the dietary guidelines for Americans, 1980–2015. Adv. Nutr. *9*, 148–150.

Palm, W., and Thompson, C.B. (2017). Nutrient acquisition strategies of mammalian cells. Nature *546*, 234–242.

Serini, S., Ottes Vasconcelos, R., Fasano, E., and Calviello, G. (2016). How plausible is the use of dietary n-3 PUFA in the adjuvant therapy of cancer? Nutr. Res. Rev. *29*, 102–125.

Shimada, K., Hayano, M., Pagano, N.C., and Stockwell, B.R. (2016). Cell-line selectivity improves the predictive power of pharmacogenomic analyses and helps identify NADPH as biomarker for ferroptosis sensitivity. Cell Chem. Biol. *23*, 225–235.

Snaebjornsson, M.T., Janaki-Raman, S., and Schulze, A. (2020). Greasing the wheels of the cancer machine: the role of lipid metabolism in cancer. Cell Metab *31*, 62–76.

Steck, S.E., and Murphy, E.A. (2020). Dietary patterns and cancer risk. Nat. Rev. Cancer *20*, 125–138.

Sullivan, M.R., Danai, L.V., Lewis, C.A., Chan, S.H., Gui, D.Y., Kunchok, T., Dennstedt, E.A., Vander Heiden, M.G., and Muir, A. (2019). Quantification of microenvironmental metabolites in murine cancers reveals determinants of tumor nutrient availability. eLife *8*, e44235.

Tajan, M., and Vousden, K.H. (2020). Dietary approaches to cancer therapy. Cancer Cell *37*, 767–785.

Ubellacker, J.M., Tasdogan, A., Ramesh, V., Shen, B., Mitchell, E.C., Martin-Sandoval, M.S., Gu, Z., McCormick, M.L., Durham, A.B., Spitz, D.R., et al. (2020). Lymph protects metastasizing melanoma cells from ferroptosis. Nature *585*, 113–118.

Van Blarigan, E.L., Fuchs, C.S., Niedzwiecki, D., Ye, X., Zhang, S., Song, M., Saltz, L.B., Mayer, R.J., Mowat, R.B., Whittom, R., et al. (2018). Marine omega-3 polyunsaturated fatty acid and fish intake after colon cancer diagnosis and survival: CALGB 89803 (Alliance). Cancer Epidemiol. Biomarkers Prev. *27*, 438–445.

van der Meij, B.S., Langius, J.A., Spreeuwenberg, M.D., Slootmaker, S.M., Paul, M.A., Smit, E.F., and van Leeuwen, P.A. (2012). Oral nutritional supplements containing n-3 polyunsaturated fatty acids affect quality of life and functional status in lung cancer patients during multimodality treatment: an RCT. Eur. J. Clin. Nutr. *66*, 399–404.

Vander Heiden, M.G., and DeBerardinis, R.J. (2017). Understanding the intersections between metabolism and cancer biology. Cell *168*, 657–669.

Viswanathan, V.S., Ryan, M.J., Dhruv, H.D., Gill, S., Eichhoff, O.M., Seashore-Ludlow, B., Kaffenberger, S.D., Eaton, J.K., Shimada, K., Aguirre, A.J., et al. (2017). Dependency of a therapy-resistant state of cancer cells on a lipid peroxidase pathway. Nature *547*, 453–457.

Xia, S., Lin, R., Jin, L., Zhao, L., Kang, H.-B., Pan, Y., Liu, S., Qian, G., Qian, Z., Konstantakou, E., et al. (2017). Prevention of dietary-fat-fueled ketogenesis attenuates BRAF V600E tumor growth. Cell Metab *25*, 358–373.

Yen, C.L., Stone, S.J., Koliwad, S., Harris, C., and Farese, R.V., Jr. (2008). Thematic review series: glycerolipids. DGAT enzymes and triacylglycerol biosynthesis. J. Lipid Res. *49*, 2283–2301.

Zhang, Y., Tan, H., Daniels, J.D., Zandkarimi, F., Liu, H., Brown, L.M., Uchida, K., O'Connor, O.A., and Stockwell, B.R. (2019). Imidazole ketone erastin induces ferroptosis and slows tumor growth in a mouse lymphoma model. Cell Chem. Biol. *26*, 623–633.e9.

Zick, S.M., Snyder, D., and Abrams, D.I. (2018). Pros and cons of dietary strategies popular among cancer patients. Oncology (Williston Park) *32*, 542–547.

Please cite this article in press as: Dierge et al., Peroxidation of n-3 and n-6 polyunsaturated fatty acids in the acidic tumor environment leads to ferroptosis-mediated anticancer effects, Cell Metabolism (2021), https://doi.org/10.1016/j.cmet.2021.05.016

STAR★METHODS

KEY RESOURCES TABLE

REAGENT or RESOURCE	SOURCE	IDENTIFIER
Antibodies		
Mouse monoclonal anti-β-Actin	Merck	Cat# A5441; RRID: AB_476744
Mouse monoclonal anti-4-Hydroxy-2-hexenal (6F10)	Novus Biologicals	Cat# NBP2-59352
Mouse monoclonal anti-CD36 [FA6-152]	Abcam	Cat# Ab17044; RRID: AB_443600
Mouse monoclonal anti-CD36 [JC63.1]	Abcam	Cat# Ab23680; RRID: AB_447608
Rabbit polyclonal anti-Caspase-3	Cell Signaling Technology	Cat# 9662; RRID: AB_331439
Rabbit polyclonal anti-Cleaved Caspase-3 (Asp175)	Cell Signaling Technology	Cat# 9661; RRID: AB_2341188
Rabbit polyclonal anti-DHFR	Cell Signaling Technology	Cat# 45710
Rabbit polyclonal anti-DGAT1	Abcam	Cat# Ab54037; RRID: AB_2090799
Rabbit polyclonal anti-FSP1	Proteintech	Cat# 20886-1-AP
Rabbit polyclonal anti-GPX4	Cell Signaling Technology	Cat# 52455
Rabbit polyclonal anti-Malondialdehyde	Abcam	Cat# Ab6463; RRID: AB_305484
Rabbit polyclonal anti-SLC7A11	Thermo Fisher Scientific	Cat# PA1-16893; RRID: AB_2286208
Goat anti-mouse IgG (H+L) highly cross-adsorbed secondary antibody, Alexa Fluor 568	Thermo Fisher Scientific	Cat# A-11031; RRID: AB_144696
Goat anti-rabbit IgG (H+L) highly cross-adsorbed secondary antibody, Alexa Fluor 568	Thermo Fisher Scientific	Cat# A-11036; RRID: AB_10563566
Bacterial and virus strains		
Edit-R Lentiviral hEF1α-Blast-Cas9 Nuclease vector particles	Dharmacon	Cat# VCAS10126
DGAT1-targeting sgRNA	Dharmacon	Cat# VSGH10142
Chemicals, peptides, and recombinant proteins		
1,2-dipentadecanoyl-sn-glycero-3-phosphatidylcholine	Larodan	Cat# 37-1500
A922500 (DGAT1 inhibitor)	Merck	Cat# A1737
Alexa Fluor 568-conjugated pH-low insertion peptide variant 3	Thermo Fisher Scientific	N/A
Arachidonic acid	Larodan	Cat# 10-2004
C_{11}-BODIPY$^{581/591}$	Thermo Fisher Scientific	Cat# D3861
DAPI	Merck	Cat# D9542
D-glucose	Merck	Cat# G8270
Docosahexaenoic acid	Larodan	Cat# 10-2206
Docosapentaenoic acid (n-6)	Larodan	Cat# 10-2265
Dulbecco's Modified Eagle's Medium (DMEM)	Merck	Cat# D5030
Eicosapentaenoic acid	Larodan	Cat# 10-2005
Erastin	Selleckchem	Cat# S7242
Ferrostatin-1	Selleckchem	Cat# S7243
Fetal Bovine Serum	Merck	Cat# F7524
FITC-conjugated Annexin V	Immunostep	Cat# ANXVF-200T
Fluorescence Mounting Medium	Dako	Cat# S3023
Free-fatty acid bovine serum albumin	Merck	Cat# A7030
Hematoxylin	Dako	Cat# S3301

(*Continued on next page*)

Please cite this article in press as: Dierge et al., Peroxidation of n-3 and n-6 polyunsaturated fatty acids in the acidic tumor environment leads to ferroptosis-mediated anticancer effects, Cell Metabolism (2021), https://doi.org/10.1016/j.cmet.2021.05.016

Continued

REAGENT or RESOURCE	SOURCE	IDENTIFIER
HEPES	Merck	Cat# H3375
L-glutamine	Thermo Fisher Scientific	Cat# 25030024
Liproxstatin-1	Selleckchem	Cat# S7699
Liquid Captisol	Captisol	Cat# LC-0C7-250
Linoleic acid	Larodan	Cat# 10-1802
Linolenic acid	Larodan	Cat# 10-1803
Methyl Undecanoate	Larodan	Cat# 20-1100
Oil red O	Merck	Cat# O0625
Oleic acid	Larodan	Cat# 10-1801
Palmitic acid	Larodan	Cat# 10-1600
PEG300	Selleckchem	Cat# S6704
PF-06424439 (DGAT2 inhibitor)	Merck	Cat# PZ0233
PIPES	Merck	Cat# P2949
PrestoBlue HS cell viability reagent	Thermo Fisher Scientific	Cat# P50201
Propidium iodide	Merck	Cat# P4170
Staurosporine	Merck	Cat# S4400
Sulfasalazine	Selleckchem	Cat# S1576
Tridecanoic acid	Larodan	Cat# 10-1300
Triheptadecanoin	Larodan	Cat# 33-1700
Trypan Blue	Thermo Fisher Scientific	Cat# 15250061
Tween 80	Selleckchem	Cat# S6702
Vitamin E (+)-α-Tocopherol	Merck	Cat# T3634
Critical commercial assays		
Bicinchoninic acid-based protein assay kit	Thermo Fisher Scientific	Cat# 23225
Lipid Peroxidation (MDA) Assay Kit	Merck	Cat# MAK085
Lipoprotein Lipase Assay Ki	Abcam	Cat# ab204721
Mouse lipopolysaccharides(LPS) ELISA kit	Mybiosource	Cat# MBS7700668
Mouse Malondialdehyde (MDA) ELISA kit	Mybiosource	Cat# MBS269473
MycoAlert mycoplasma detection kit	Lonza	Cat# LT07-318
Experimental models: Cell lines		
Human: HCT-116 cells	ATCC	Cat# CCL-247
Human: SiHa cells	ATCC	Cat# HTB-35
Human: FaDu cells	ATCC	Cat# HTB-43
Experimental models: Organisms/strains		
Rj:NMRI-Foxn1nu/nu 6-week female mice	Janvier Labs	N/A
BALB/c-nu immunodeficient 6-week mice	Janvier Labs	N/A
Software and algorithms		
ChromQuest 5.0	Thermo Fisher Scientific	N/A
FACSCanto II	BD Biosciences	N/A
Fiji	ImageJ	N/A
M3Vision	Biospace Lab	N/A

RESOURCE AVAILABILITY

Lead contact

Further information and requests for resources and reagents should be directed to and will be fulfilled by the Lead Contact, Olivier Feron (olivier.feron@uclouvain.be).

Materials availability

This study did not generate new unique reagents.

Data and code availability

The data supporting the findings of this study are available within the article and the associated **supplemental information**. This study did not generate datasets.

EXPERIMENTAL MODEL AND SUBJECT DETAILS

Cell lines & culture

Human colorectal HCT-116, hypopharyngeal FaDu and cervix SiHa cancer cell lines were purchased from ATCC. Cell lines were stored according to the supplier's instructions and used within 6 months after resuscitation of frozen aliquots. All cells were maintained in DMEM supplemented with 10% heat-inactivated FBS, 10 mM D-glucose, 2 mM L-glutamine and 25 mM of PIPES and HEPES before adjusting the pH to 7.4 or 6.5. Acid-adapted cancer cells were established as previously described (Corbet et al., 2014). All cell lines were tested for mycoplasma contamination with the MycoAlert Mycoplasma Detection kit (Lonza). Cell density was determined by using the Presto Blue reagent (Thermo Fisher Scientific) according to manufacturer's instructions. After collection, cell number was assessed by cell counting on a hemocytometer with Trypan Blue exclusion dye. For CRISPR-Cas9 system, HCT-116 cancer cells were infected with an Edit-R Lentiviral hEF1α-Blast-Cas9 Nuclease vector (VCAS10126, Dharmacon). After a one-week selection with 8 μg/mL blasticidin (ant-bl-05, InvivoGen), Cas9-expressing cells were then secondly infected with either a non-targeting single guide (sg) RNA (VSGC10215; Dharmacon), or a DGAT1-targeting sgRNA (VSGH10142-246592856; 246592860; 246995078, Dharmacon). Final selection of sgRNA-expressing cells was done with 2 μg/ml puromycin for 1 week.

Mouse strains

Experiments involving mouse xenograft received the approval of the ethic committee from UCLouvain (approval ID 2016/UCL/MD018) and were carried out according to national care regulations. All mice were fed with isocaloric croquettes (Safe) enriched with either 10% of olive oil (OA diet) or 10% of MorDHA oil (DHA diet) (kindly provided by Minami), the composition of which being detailed in Table S1. For fatty acid quantification, 6-week-old female BALB/c-nu immunodeficient mice (Janvier) were fed the OA-rich or the DHA-rich diet for 4 weeks, before sacrifice and sampling of blood and liver. For experiments evaluating tumor growth, mice were fed for 1 week either diet prior cancer cell injection and throughout the experiment. Food was renewed every 2-3 days in every experiments.

METHOD DETAILS

2D culture treatment

Each treatment was performed in a full culture medium with 2 μg/ml FA6-152 (ab1044, Abcam), 1 μg/ml JC63.1 (ab23680, Abcam), 10 μM ferrostatin-1, 10 μM liproxstatin-1 (S7699, Selleckchem), 15 μM DGAT1 inhibitor A922500 (A1737, Merck), 10 μM DGAT2 inhibitor PF-06424439 (PZ0233, Merck) or 1 μM Staurosporine (S4400, Merck). Cell growth medium was supplemented with 10, 50 or 100 μM BSA-conjugated fatty acids for 24h, 48h or 72h depending on the experiment. All fatty acids were purchased from Larodan: palmitic acid (10-1600), oleic acid (10-1801), linoleic acid (10-1802), arachidonic acid (10-2004), n-6 docosapentaenoic acid (10-2265), linolenic acid (10-1803), eicosapentaenoic acid (10-2005) and docosahexaenoic acid (10-2206). Fatty acids were conjugated with BSA in PBS as to obtain a fatty acid/BSA ratio of 4:1 (w:w). Aliquoted fatty acids were stored at -20°C under light protection (-80°C when stored for more than one week) and directly used upon unfreezing by addition of the requested concentrations into the wells.

Oil red O staining

Cells were seeded in Nunc Lab-Tek II Chamber Slide system (Merck), then treated with fatty acids, 2 μg/ml FA6-152, 1 μg/ml JC63.1, 15 μM DGAT1 inhibitor or 10 μM DGAT2 inhibitor for 24h. Cells were washed 2 times with PBS, then fixed with 4% (w:v) paraformaldehyde for 20 minutes before staining with 3 mg/mL Oil Red O solution in 60% isopropanol (v:v) for 30 minutes. After counterstain with hematoxylin, bright-field images were taken at x63 magnification using AxioImager.z1-ApoTome1 (Zeiss). Lipid droplet and nucleus areas were finally assessed with Fiji software.

Fatty acid quantification

Cells collected in PBS, serum or lyophilized liver, tumor or adipose tissue were used to determine the fatty acid concentration. Firstly, total lipids were extracted with methanol:chloroform:water (2:2:1.8; v:v:v) (Bligh and Dyer, 1959). An internal standard composed of tridecanoic acid, 1,2-dipentadecanoyl-sn-glycero-3-phosphatidylcholine and triheptadecanoin (Larodan) was added in each sample to evaluate the extraction yields and control the separation between free fatty acids, phospholipids and neutral lipids, respectively. Samples were dried under a stream of nitrogen at 30°C and resuspended in chloroform. Secondly, resuspended lipids were loaded on solid phase extraction columns (Bond Elut-NH_2, 200 mg, 3mL) (Agilent Technologies) and neutral lipid, free fatty acid and phospholipid fractions were eluted with chloroform:2-propanol (2:1; v:v); diethyl ether:acetic acid (98:2; v:v) and methanol, respectively. Thirdly, samples were dried and methylated under alkaline conditions (KOH 0.1M in methanol at 70°C for 1 h) and then under acidic conditions (HCl 1.2M in methanol at 70°C for 15 min). Fatty acid methyl esters (FAMEs) were extracted with hexane. Fourthly, methyl-undecanoate (Larodan) was added in each sample as an injection standard. FAMEs were injected and separated by gas chromatography

(Trace 1310) (Thermo Fisher Scientific) equipped with an autosampler TriPlusAS and a RT-2560 capillary column (biscyanopropylpolysiloxane 100 m length, 0.25 mm internal diameter, 0.2 μm film thickness; Restek), continuously flowed with H_2 as a carrier gas at a constant pressure of 200 kPa. The GC temperature program was the following: an initial temperature of 80°C which increased to 175°C (for 25 min) at 25°C/min, then to 200°C (for 20 min) at 10°C/min, then to 220°C (for 5 min) at 10°C/min and finally to 235°C (for 15 min) at 10°C/min. Finally, temperature decreased down to 80°C at 20°C/min. FAMEs were detected using a flame ionizing detector kept at a constant temperature of 255°C and flowed by air (350 mL/min), H_2 (35mL/min) and N_2 (40 mL/min). An external standard composed of 43 pure methyl ester standards (Larodan and Nu-Check Prep) was used to identify the unknown peaks with the retention time and to quantify the peaks through the known concentrations. Chromatographs were processed by using ChromQuest 5.0 software (Thermo Fisher Scientific). Results are expressed in nmol of FA per million of cells or per μmol of FA in 1 liter of serum, total liver or 100mg of dry subcutaneous white adipose tissue after data normalization with the internal standard (percentage of recovery), the injection standard, the starting cell number or the organ weight.

3D spheroid models

Spheroids were formed with 7.4/HCT-116 or FaDu cells seeded at a density of 1,000 cells/well in 96-well ultra-low attachment plates (Corning) in pH 7.4 DMEM supplemented with 10% heat-inactivated FBS, 10 mM D-glucose, 2 mM L-glutamine and 25 mM of PIPES and HEPES. Spheroids were treated with 10, 25, 50 or 100 μM fatty acid, growing pH medium, medium without PIPES and HEPES but with 22 mM bicarbonate, 15 μM DGAT1 inhibitor, 10 μM DGAT2 inhibitor, 0.2 or 1 μM (+)-α-Tocopherol (Vitamin E) (T3634 Merck), 0.5 μM erastin, 5 μM ferrostatin-1 or 5 μM liproxstatin-1 3 days after seeding (day 0). Afterwards, the treatment was renewed every 2 or 3 days. Spheroid growth was monitored using live-cell phase contrast microscope (Axio Observer, Zeiss) and spheroid area was measured by Fiji software. For immunofluorescence staining, spheroids were incubated for 24h with 2 μM Alexa Fluor 568-conjugated pH-low insertion peptide variant 3 (pHLIP V3) or for 15 minutes with 1mg/mL propidium iodide (P4170 Merck). Afterwards, 3-day or 7-day old spheroids were harvested, fixed with 4% PFA, incubated with 30% sucrose and finally embedded in OCT. Frozen sections (7 μm) were counterstained with DAPI. Slides were prepared with fluorescence mounting medium (Dako) and the staining was visualized by AxioImager.z1-ApoTome1 (Zeiss). All spheroid samples from a same experiment were imaged with the same gain and exposure settings.

MDA measurements

Malondialdehyde concentration in cellular extracts was determined with the Lipid Peroxidation (MDA) Assay Kit from Merck (MAK085), according to manufacturer's instructions. Malondialdehyde concentration in mouse serum was determined with the Mouse malondialdehyde (MDA) ELISA kit from Mybiosource (MBS269473), according to manufacturer's instructions.

Peroxidation potential

Cells were seeded in a Corning 96-well black/clear bottom plate (3614 Corning). Peroxidation potential was assessed using a fluorescent lipid probe C_{11}-BODIPY$^{581/591}$ (4,4-difluoro-5-(4-phenyl-1,3-butadienyl)-4bora-3a,4a-diaza-s-indacene-3-undecanoic acid, D3861 Thermo Fisher Scientific) provided with 2 double bonds that are oxidized in the presence of ROS. Upon excitation, the probe color changes from non-peroxidized: red to peroxidized: green. Cells were incubated with 3 μM of C_{11}-BODIPY$^{581/591}$ for 30 min at 37°C. Then, cells were washed and the red and green fluorescence levels were evaluated using a Spectramax microplate reader (Molecular Devices) (red: $\lambda_{excitation}$=485 nm, $\lambda_{emission}$=520 nm; green: $\lambda_{excitation}$=485 nm and $\lambda_{emission}$=595 nm). Data are expressed as relative fluorescence units related to the green fluorescence divided by the red fluorescence.

Flow cytometry

For cell death profiling, cells were treated with fatty acid or staurosporine as indicated. After treatment, adherent and floating cells were collected and washed with PBS. Cells were consecutively incubated with FITC-conjugated Annexin V (ANXVF-200T, Immunostep) and 1 μg/mL propidium iodide for 15 min at room temperature in the dark. After incubation, cells were analyzed by flow cytometry on FACSCanto II (BD Biosciences) with a gating strategy excluding debris and doublet cells.

Western blot

Cancer cell monolayers were washed twice with PBS and lysed in a RIPA buffer supplemented with a protease inhibitor cocktail. Cells from supernatant were also collected. Protein concentration was determined on cell lysates using a bicinchoninic acid-based assay (Thermo Fisher Scientific). Samples were then denaturated (7 min, 95°C) with Laemmli sample buffer containing 100 mM dithiothreitol. Afterwards, samples (20 μg per well) were separated by SDS-PAGE (15% acrylamide/bis-acrylamide gels) and transferred to PVDF membranes. Membranes were then blocked with 5% skimmed milk for GPX4 (52455, Cell Signaling Technology, 1:1000), SLC7A11 (A1-16893, Thermo Fisher Scientific, 1:1000), FSP1 (20886-1-AP, Proteintech, 1:500), DHFR (45710, Cell Signaling Technology, 1:1000), Caspase-3 (9662, Cell Signaling Technology, 1:1000) and Cleaved-Caspase-3 (9661, Cell Signaling Technology, 1:1000), DGAT1 (ab54037, Abcam, 1:2000) and 5% BSA for β-actin (A5441, Merck, 1:10000) in TBS-0.1% Tween 20 (TTBS) and subsequently immunoblotted overnight at 4°C with the specific primary antibody. After several washes with TTBS, membranes were incubated 1h at room temperature with horseradish peroxidase (HRP)-conjugated secondary antibodies (Jackson Immunoresearch) and chemoluminescent signals were revealed by using ECL Western Blotting Detection Kit (GE Healthcare) on X-ray films in a dark chamber.

Oxygen-consumption rate measurements

Oxidation of exogenous fatty acids was assessed by treating cancer cells with indicated FA after one night deprivation in a substrate-limited medium. Oxygen-consumption rate (OCR) was measured before and after addition of etomoxir using the Seahorse XF96 plate reader (Agilent Technologies).

In vivo mouse experiment

Before injection in Rj:NMRI-Foxn1nu/nu 6-week female mice, 7.4/HCT-116 cancer cells were washed twice with PBS, resuspended in 0.9% NaCl and $2x10^6$ cells were injected in the right flank of each mouse. When tumors reached 60 to 100 mm^3, mice were treated daily with DGAT1 inhibitor (3 mg/kg) in 15% Captisol by oral dosing or with sulfasalazine (S1576, Selleckchem) (150 mg/kg) in 5% DMSO, 40% PEG300, 5% Tween80 and 50%% water, with ferrostatin-1 (S7243, Selleckchem) (20 mg/kg) in 2% DMSO, 50% PEG300, 5% Tween80 and 43% water or with erastin (S7242, Selleckchem) (15 mg/kg) in 5% DMSO, 40% PEG300, 5% Tween80 and 50% water by daily intraperitoneal injection. Control groups were treated in parallel with equivalent vehicles. Mice were weighed and tumors were measured 3 times a week. At the end of experiment, when tumor size reached the ethical endpoint, mice were sacrificed and tumors were collected. A precise adipose tissue harvest was performed as detailed elsewhere (Bagchi and MacDougald, 2019), to retrieve and weigh the brown, the subcutaneous anterior, the subcutaneous posterior and the visceral white adipose tissues. Collected tumors were fixed with 4% paraformaldehyde for 48h, incubated with 30% sucrose for 48 hours and finally embedded in OCT. Frozen sections (5μm) on slides were used to perform immunohistofluorescent stainings. After blocking with 5% BSA for 1h, tumor sections were incubated overnight at 4°C with anti-MDA (ab6463, Abcam, 1:500) or anti-4HHE (NBP2-59352, Novus Biologicals, 1:50) antibody. Sections were then incubated with Alexa Fluor 568-conjugated anti-rabbit (A11036, Thermo Fisher Scientific, 1:500) or anti-mouse (A11031, Thermo Fisher Scientific, 1:500) secondary antibody for 1h, respectively. Finally, nuclei were counterstained with DAPI and slides were prepared with fluorescence mounting medium (Dako). The staining was visualized by AxioImager.z1-ApoTome1 (Zeiss). All tumor samples were imaged with the same gain and exposure settings. 40 μM Alexa647-conjugated pHLIP peptide and 40 μM pH-independent control Alexa568-conjugated K-pHLIP peptide were co-injected in HCT-116 tumor-bearing mice and fluorescence pictures were taken after 24 hours with PhotonIMAGER (Biospace Lab). The pictures were analyzed with M3Vision software. Finally, mouse serum components were measured through mouse lipopolysaccharides (LPS) ELISA kit (MBS7700668, Mybiosource) and through dry chemistry analyzer for AST, ALT and BUN (Fuji Dri-Chem slide, Fujifilm).

QUANTIFICATION AND STATISTICAL ANALYSIS

Statistical analyses were performed through GraphPad Prism 7 by using Student's t test, one-way ANOVA with Tukey's multiple comparison test, two-way ANOVA with Tukey's or Sidak's multiple comparison test or with log-rank (Mantel-Cox) test when appropriate. Statistical significance is indicated in the Figures as follows: *$p < 0.05$; **$p < 0.01$; ***$p < 0.001$.